1 Research article

- 2 Posttranslational modification of the NADP-malic enzyme involved in C₄ photosynthesis
- 3 fine-tunes the enzymatic activity during the day
- 4 Anastasiia Bovdilova¹, Bruno M. Alexandre^{2,3}, Astrid Höppner⁴, Inês Matias Luís², Clarisa E.
- 5 Alvarez⁵, David Bickel⁶, Holger Gohlke^{6,7}, Christina Decker⁸, Luitgard Nagel-Steger⁸, Saleh
- 6 Alseekh^{9,10}, Alisdair R. Fernie^{9,10}, Maria F. Drincovich⁵, Isabel A. Abreu^{2,3}, Veronica G.
- 7 Maurino¹,*
- 8 Institute of Developmental and Molecular Biology of Plants, Plant Molecular Physiology and
- 9 Biotechnology Group, Heinrich Heine University Düsseldorf, Universitätsstraße 1, and
- 10 Cluster of Excellence on Plant Sciences (CEPLAS), 40225 Düsseldorf, Germany.
- ²Instituto de Biologia Experimental e Tecnológica, Avenida da República, Quinta do
- 12 Marquês, 2780-157 Oeiras, Portugal.
- ³Instituto de Tecnologia Química e Biológica António Xavier, Universidade Nova de Lisboa,
- 14 Avenida da República, 2780-157 Oeiras, Portugal.
- 15 ⁴Center for Structural Studies (CSS), Heinrich Heine University Düsseldorf,
- 16 Universitätsstraße 1, 40225 Düsseldorf, Germany.
- 17 ⁵Centro de Estudios Fotosinteticos y Bioquimicos (CEFOBI-CONICET), Facultad de
- 18 Ciencias Bioquímicas y Farmacéuticas, University of Rosario, Suipacha 570, 2000 Rosario,
- 19 Argentina.
- 20 ⁶Institute for Pharmaceutical and Medicinal Chemistry, Heinrich Heine University
- Düsseldorf, Universitätsstraße 1, 40225 Düsseldorf, Germany.
- ⁷John von Neumann Institute for Computing (NIC), Jülich Supercomputing Centre (JSC) &
- 23 Institute for Complex Systems Structural Biochemistry (ICS 6), Forschungszentrum Jülich
- 24 GmbH, 52425 Jülich, Germany
- 25 ⁸Institut für Physikalische Biologie, Heinrich Heine University Düsseldorf, Universitätsstraße
- 26 1, 40225 Düsseldorf, Germany and Institute of Complex Systems, Structural Biochemistry
- 27 (ICS-6), Forschungszentrum Jülich, 52425 Jülich, Germany.
- ⁹Max-Planck-Institute of Molecular Plant Physiology, Am Mühlenberg 1, 14476 Potsdam-
- 29 Golm, Germany.
- 30 ¹⁰Center for Systems Biology and Biotechnology, 4000 Plovdiv, Bulgaria.
- * Corresponding Author: veronica.maurino@uni-duesseldorf.de

33 **Short Title:** *In vivo* phosphorylation of maize C₄-NADP-ME

One-sentence summary: Phosphorylation of ZmC₄-NADP-ME at S419 decreases the binding affinity to NADP fine-tuning the enzymatic activity during the first hours in the light.

32

- 38 The author responsible for distribution of materials integral to the findings presented in this
- 39 article in accordance with the policy described in the Instructions for Authors
- 40 (www.plantcell.org) is: Veronica G. Maurino (veronica.maurino@uni-duesseldorf.de).

41 ABSTRACT

- 42 Evolution of the C₄ photosynthetic pathway involved in some cases recruitment of
- 43 housekeeping proteins through gene duplication and their further neofunctionalization.
- NADP-malic enzyme (ME), the most widespread C₄ decarboxylase, has increased its catalytic
- 45 efficiency and acquired regulatory properties that allowed it to participate in the C₄ pathway.
- 46 Here, we show that regulation of maize C₄-NADP-ME activity is much more elaborated than
- 47 until now indicated. Using mass spectrometry, we identified phosphorylation of the serine 419
- 48 (S419) of C₄-NADP-ME in protein extracts of maize leaves. The phosphorylation event
- 49 increases after the light turns on, with a peak at ZT2. Phosphorylation of ZmC₄-NADP-ME
- drastically decreases its activity as shown by the low residual activity of the recombinant
- 51 phosphomimetic mutant. Analysis of the crystal structure of C₄-NADP-ME indicated that
- 52 S419 is involved in the binding of NADP at the active site. Molecular dynamics simulations
- and effective binding energy computations indicate a less favorable binding of the cofactor
- 54 NADP in the phosphomimetic and the phosphorylated variants. We propose that
- phosphorylation of ZmC₄-NADP-ME at S419 during the first hours in the light is a cellular
- 56 mechanism to fine-tune the enzymatic activity to coordinate the carbon concentration
- 57 mechanism with the CO₂ fixation rate, most probably to avoid CO₂ leakiness from bundle
- sheath cells.

59

60

INTRODUCTION

- 61 The world's most productive crops perform C₄ photosynthesis. The ancestors of these plants
- evolved a biochemical pump to concentrate CO₂ at the site of Rubisco leading to lower
- 63 photorespiratory fluxes and greater photosynthetic efficiency (Furbank and Hatch, 1987).
- 64 Compared with the ancestral C₃ photosynthesis, the C₄ pathway allows increased plant
- productivity in warm habitats due to a more efficient use of nitrogen and water.
- The most agronomically important C₄ plants maize, sorghum, and sugar cane belong to the
- NADP-ME subtype. In these plants, CO₂ is initially fixed in the mesophyll cells by
- 68 phosphoenolpyruvate carboxylase (PEPC), leading to the formation of oxaloacetate.
- 69 Oxaloacetate is then predominantly reduced to malate and transported into the bundle sheath
- 70 cells (BSC), where CO₂ is released by NADP-malic enzyme (NADP-ME) for its refixation

through Rubisco (Hatch, 1987). By this process, CO₂ concentration in the BSC rises to levels

72 up to 1,500 μ L L⁻¹ (Furbank and Hatch, 1987;Sage et al., 2012).

87

88

89

90

91

92

93

94

95

96

97

98

99

100

101

102

103

73 The transition from C₃ to C₄ metabolism involved complex alterations to leaf anatomy and 74 biochemistry. A crucial step in the evolution of the C₄ photosynthetic pathway was the recruitment of some enzymes through gene duplication of housekeeping isoforms and 75 76 subsequent neofunctionalization. In the course of its evolution, the C₄-specific NADP-ME 77 isoform increased its catalytic efficiency and acquired regulatory properties that optimized its 78 efficiency in the C₄ pathway (Saigo et al., 2013; Alvarez et al., 2019). During the night, when 79 the delivery of malate from the PEPC reaction is stopped, C₄-NADP-ME activity is inhibited 80 by malate (Saigo et al., 2004; Saigo et al., 2013). This property, exclusive to the C₄ isoform, 81 minimizes the malate consumption to avoid extreme carbon loss during the night period, 82 which would otherwise result in carbon starvation (Fahnenstich et al., 2007; Zell et al., 2010). 83 At the pH of the stroma in darkness, a proportion of C₄-NADP-ME likely loses its quaternary 84 structure and adopts a lower oligomerization state that is less active or even inactive (Iglesias 85 and Andreo, 1990). This likely represents a second level of regulation that ensures that C₄-86 NADP-ME is less active during the night period.

The enzymatic activities of some enzymes of C₄ metabolism and also of the CAM carbon concentrating pathway are known to be regulated through post-translational modifications (PTMs). PTMs provide mechanisms for rapid and reversible control of activity of these proteins in a coordinated fashion during the day and night and in response to light intensity (Walker et al., 2002; Bailey et al., 2007; Chen et al., 2014). The activity of C₄-PEPC is regulated through phosphorylation of a serine residue located at the N-terminal region by a small PEPC kinase (PEPC-PK) (Nimmo, 2003). C₄-PEPC is mainly phosphorylated in the light, where it has a higher catalytic activity and is less sensitive to the allosteric inhibition by malate than in darkness (Jiao and Chollet, 1988;1989;1990). Transgenic lines of Flaveria bidentis with antisense or RNA interference constructs targeted at the mRNA of the PEPC-PK demonstrated that the kinase is essential for the phosphorylation of C₄-PEPC in vivo (Furumoto et al., 2007). In the transgenic lines C₄-PEPC was not phosphorylated in the light, nevertheless no differences in the CO₂ and light response of CO₂ assimilation rates between them and the wild type (Furumoto et al., 2007). These results suggest that phosphorylation of PEPC in the light is not essential for efficient C₄ photosynthesis in plants grown under standard glasshouse conditions but it remains to be determined if photosynthetic rates are affected under stress conditions.

104 PEPC of the obligate CAM species Kalanchoë fedtschenkoi is also regulated by 105 phosphorylation (Hartwell et al., 1999; Nimmo, 2000). A specific PEPC kinase phosphorylates 106 CAM-PEPC during the dark period, reducing its sensitivity to feedback inhibition by malate, 107 enabling nocturnal fixation of CO₂ into malate (Boxall et al., 2017). C₄-pyruvate 108 orthophosphate dikinase (C₄-PPDK) activity, in contrast, is not controlled by the light/dark 109 transition per se but rather by the light intensity. In this case, increased phosphorylation takes 110 place with waning light intensity in the evening leading to a decrease in activity (Chen et al., 111 2014). C₄-PPDK is regulated by reversible phosphorylation of a threonine residue of the 112 active site (Burnell and Hatch, 1985; Chastain et al., 2000) catalyzed by the PPDK regulatory protein (PDRP) (Chen et al., 2014). PDRP is bifunctional; it catalyzes both PPDK 113 114 activation/dephosphorylation and PPDK inactivation/phosphorylation (Burnell and Chastain, 115 2006; Chastain et al., 2008; Astley et al., 2011). The regulatory phosphorylation of C₄-PPDK is 116 a very ancient mechanism as genes coding for PDRP are present in C₃ plants and prokaryotes 117 (Agarie et al., 1997;Imaizumi et al., 1997;Wei et al., 2000;Burnell, 2010). In some C₄ plants 118 such as Guinea grass (Panicum maximum) and maize, PEP carboxykinase (C₄-PEPCK) is 119 phosphorylated in the dark when the enzyme is less active, and dephosphorylated under 120 illumination (Walker and Leegood, 1996; Walker et al., 2002; Chao et al., 2014). 121 Modifications in the phosphorylation state of PEPCK lead to changes in its sensitivity to 122 adenylates, which would be involved in the activation of the enzyme in the light (Walker et 123 al., 2002). Recently, it was shown that phosphorylation of a serine residue in maize C₄-124 PEPCK is also dependent on the light regime (Chao et al., 2014). 125 Little is known about the participation of PTMs in the regulation of the C₄-NADP-ME

Little is known about the participation of PTMs in the regulation of the C₄-NADP-ME isoform *in vivo*. Until now, only the effects of redox modulation on the recombinant ZmC₄-NADP-ME activity were reported (Alvarez et al., 2012). Oxidation of ZmC₄-NADP-ME decreases the catalytic activity and increases the affinity for malate and the cofactor; in combination, these changes produce no significant changes of the catalytic efficiency. The oxidation of C192, C246, C270 and C410 may contribute to the changes observed *in vitro* (Alvarez et al., 2012).

132

133

134

135

136

137

Here, we show a novel PTM, phosphorylation at S419, of ZmC₄-NADP-ME, which takes place *in vivo* after the light is turned on, with a peak at 2 h after the onset of light. The results of the characterization of the recombinant phosphomimetic mutant S419E together with the analysis of the crystal structure of C₄-NADP-ME, and molecular modeling and dynamic simulations of wild-type and mutant enzymes indicate that phosphorylation at S419 inactivates ZmC₄-NADP-ME because S419 is involved in NADP binding at the active site.

We postulate that the novel PTM of ZmC₄-NADP-ME described here is a mechanism to finetune the enzymatic activity, most probably to coordinate malate decarboxylation with carbon fixation in BSC.

RESULTS

Identification of a phosphorylation site in ZmC₄-NADP-ME

Mass spectrometric identification of phosphorylation sites in complex protein extracts faces several challenges. Phosphopeptides are often of low abundance and often exhibit low MS signals and inadequate fragmentation patterns. To overcome these issues and to be able to identify phosphorylated peptides of ZmC₄-NADP-ME in cell lysates obtained from maize leaf macerates, we loaded maize protein extracts onto 4-12% NuPAGE gels and electrophoresed them for a short time. Upon in-gel digestion, samples were subjected to a phosphopeptide enrichment step and analyzed by LC-MS using an AB Sciex TripleTOF 6600 mass spectrometer. The acquired data was analyzed with Protein Pilot 5.0 and PeakView 2.2. This approach was successful in unambiguously detecting the phosphorylation of ZmC₄-NADP-ME at a single amino acid residue, S419. Figure 1 shows a tandem MS spectrum of the obtained peptide acVWLVDpSK. The quality of the MS/MS data for this peptide enabled the correct assignment of the phosphorylated residue. In fact, with the exception for the y₁-ion, the entire y-ion series of the peptide was assigned, and the loss of the phosphate group (H₃PO₄), corresponding to a mass-to-charge ratio of 98, was detected for the whole y-ion series.

The MS analysis did not identify any phosphorylation event in the other maize NADP-ME isoforms, as the V414 from the identified phosphorylated peptide is unique to the ZmC₄NADP-ME (Alvarez et al., 2013). We conclude that a functional role for this phosphorylation site most probably represents a C₄-trait. We next compared the protein sequences of plastidic photosynthetic and non-photosynthetic NADP-ME isoforms within the Panicoideae subfamily of the Poaceae. This sequence alignment indicated that the serine corresponding to amino acid position 419 in the C₄-NADP-ME protein sequence is conserved among all NADP-ME sequences analyzed (Supplemental Figure 1).

Production of the phosphomimetic mutant and characterization of the biochemical

properties

170 In order to analyse the effect of phosphorylation of S419 on the biochemical properties of 171 ZmC₄-NADP-ME, we generated the phosphomimetic mutant S419E by changing the S419 to 172 E by site-directed mutagenesis. Phosphorylation adds negative charge to amino acids, and 173 thus the negatively charged amino acid E can be used to mimic the phosphorylated state of a 174 protein (Dissmeyer and Schnittger, 2011). In order to assess the importance of the amino acid 175 position for the enzymatic activity, we also created the S419A variant by changing the Ser419 176 for A, a small non-polar amino acid. 177 ZmC₄-NADP-ME wild-type (WT), S419E, and S419A were heterologously expressed and 178 purified to homogeneity by affinity chromatography. The recombinant proteins, showing in 179 all cases the expected molecular masses (Supplemental Figure 2), were subjected to a 180 comparative analysis of their enzymatic properties. Analysis of the dependence of the 181 enzymatic activity on the pH of the reaction media indicated that while the recombinant WT

182 ZmC₄-NADP-ME has a pH optimum of 8.0, the S419E variant presents a shift of the pH

optimum towards more acidic pHs between 6.5 and 7.0 (Figure 2A). The S419A variant

showed a pH optimum of 7.0 - 7.5 (Figure 2A). At the physiologically relevant pH 8.0 of the

photosynthetically active stroma, the S419E variant presents only 8.7% of the WT activity,

while the S419A variant retains a 72.3% of the WT activity (Figure 2A).

187 Analysis of the affinity to NADP indicated that the exchange of the S residue for E in the

188 S419E variant dramatically decreases the affinity of the mutant for the cofactor, as saturation

was not observed even at NADP concentrations as high as 5 mM. The S419A variant

presented a 13-fold lower affinity ($K_{\rm m}$ 159.5 μM) for the cofactor in comparison to the WT

191 $(K_m 12.3 \mu M)$ (Figure 2B), indicating that S419 is essential for the normal operation of the

192 enzyme.

189

190

193

194

195

196

197

198

199

200

The affinity for the substrate malate at pH 8.0 of the WT and S419A was measured at saturating NADP concentrations. As we found that S419E is not saturated by NADP even at very high concentrations, the K_{mapp} was determined at a sub-saturating concentration of the cofactor. In comparison to the WT (K_{m} 0.19 mM), the apparent affinity for malate decreased by approximately 14-fold in the S419E variant (K_{mapp} 2.68 mM) and only 2-fold in the S419A variant (K_{m} 0.47 mM). The turnover number (k_{cat}) was measured at pH 8.0, at saturating levels of malate, and at 0.5 mM NADP. Under these conditions, the S419E variant displayed a 6-fold lower catalytic activity (k_{catapp} 2.1 s⁻¹) with respect to the WT (k_{cat} 12.2 s⁻¹) (Figure 2P). In contrast, the k_{m} of the S410A variant (k_{m} 8.3 s⁻¹) was in the same range as that of the

201 2B). In contrast, the k_{cat} of the S419A variant ($k_{\text{cat}} 8.3 \text{ s}^{-1}$) was in the same range as that of the

WT (Figure 2B).

Structural organization of the mutant variants

As the phosphomimetic mutant showed dramatic changes of its kinetic properties in comparison to the WT enzyme, we analysed if these could be the result of alterations in the structural organisation of the engineered protein. We used circular dichroism (CD) to explore the secondary structure organization and analytical ultracentrifugation (AUC) to explore the quaternary composition.

CD measurements at both pH 7.0 and 8.0 indicated no significant changes in the secondary structure organization of the mutated variants in comparison to the WT (Figure 3A and B). The data obtained indicated that ZmC₄-NADP-ME WT and the S419E and S419A variants presented similar fractions of different types of secondary structures depending on the pH. At pH 8.0, all enzymes possess almost twice the amount of helical structures observed at pH 7.0, an approximately 1.5-fold lower amount of β -strand structures, an almost unchanged amount of turns, and an only slightly decreased amount of unordered secondary structures (Supplemental Figure 4 and Supplemental Table 1). As shown in Supplemental Figure 4 for the case of the WT, the higher signal at 195 nm together with the more pronounced minimum at 208 nm is indicative of an overall increase in α -helical structure at pH 8. The decrease of beta-strand structure is hardly visible directly in the spectra, since the CD-effect of β -strand structure is lower than that of α -helix. This is why slight changes are less visible.

A comparison of the analysis presented in Supplemental Table 1 with the secondary structure determined from the crystal structure of ZmC₄-NADP-ME (pdb-code: 5OU5; (Alvarez et al., 2019)) indicates that the total helix content measured by CD increases with the pH from 24% at pH 7.0 to 37% at pH 8.0. The increase in helical structure is achieved mainly at the expense of total β-strand conformation, which decreases from 28% at pH 7.0 to 20% at pH 8.0. The change in the fractions of turn and unordered conformations is less pronounced. In comparison the crystal structure of ZmC₄-NADP-ME has 46% β-helical structure and about 11% β-strand conformation. While obviously the change in pH has a significant impact on the conformation of the protein, the structure measured by CD at pH 8.0 is more similar to the crystal structure than the measured at pH 7.0. That the structure of a protein in solution differs from its crystal structure is expected; in solution different conformational ensembles exist, while in a crystal a single conformation prevails. Additionally, different environments in solution and in the crystal and the presence or absence of the cofactor might favor different conformations. Either an ordering of the protein as the pH decreases or alterations due to

changes in domain interactions are possible causes of the deviation in secondary structure composition obtained by the different methods.

AUC measurements conducted at both pH 7.0 and 8.0 (Figure 3C and D) confirmed a stable tetrameric state of WT ZmC₄-NADP-ME at pH 8.0, with a sedimentation coefficient of 11.7 S (Figure 3D). Both mutated variants also assemble as tetramers at pH 8.0, showing sedimentation coefficients of 11.6 S and 11.1 S (Figure 3D). The sedimentation coefficient distribution of all proteins at pH 7.0 showed two peaks, with sedimentation coefficients of approximately 11.5 S and 5.4 S (Figure 3C), indicating that at this pH the enzymes exist as a mixture of monomers/dimers and tetramers with predominance of the latter. The results also indicate that the generated mutant variants have no altered quaternary structure at any pH in comparison to the WT. It can be speculated that the changes in amount of helical and turn components observed in the CD measurements at the different pHs might be related to the occurrence of a dimeric fraction at pH 7.0, as these changes may contribute to the alterations in the interface contacts between the monomers in the tetramer.

Taken together, the results of CD and AUC analyses indicate that the observed changes in the kinetic properties of the mutant variants are not due to changes in the structural organization of the proteins with respect to the WT at each pH analysed.

Diurnal profiles of ZmC₄-NADP-ME phosphorylation state, NADP-ME activity and

malate concentration in maize leaves

We quantified ZmC₄-NADP-ME total protein amount in leaves of maize at different time points during a day using SWATH-MS (sequential window acquisition of all theoretical fragment ion spectra-mass spectrometry). We found that during the day, there are no major fluctuations of the ZmC₄-NADP-ME total protein amount (Figure 4A). Following the light-to-dark transition, there is an increase in total ZmC₄-NADP-ME protein level (Figure 4A). Despite a decreasing trend over the dark period from ZT16.5 to ZT23.5, the relative levels of ZmC₄-NADP-ME to the total protein levels (as measured by SWATH-MS) are higher during

the whole dark period when compared to the light period.

Quantification of phosphorylation in S419 throughout the day indicated a significant increase of phosphorylation events after the light is turned on, with a peak at ZT2 that accounts for about 13% of the total ZmC₄-NADP-ME protein. This peak is followed by a substantial

decrease to phosphorylation levels as low as 3% at ZT4 in the light. These low levels are maintained for the remainder of the day and also during the night (Figure 4B).

Measurements of total NADP-ME activity in extracts of maize leaves indicated a slight but no significant increment of the activity between ZT2 and ZT4 in the light, followed by a constant decline during the rest of the light period (Figure 4C). The activity measured in total leaf extracts is the sum of the activity of all maize NADP-ME isoforms. As the C₄ isoform is the most highly expressed isoform in photosynthetic tissues with respect to the other isoforms (Detarsio et al., 2008;Alvarez et al., 2013), we conclude that the tendencies observed in the profile of measured NADP-ME activity represents the activity of the C₄ isoform.

We next investigated the profile of malate concentration in whole maize leaf extracts during a diurnal cycle (Figure 4D). Similar high malate concentrations were observed during the light period and at ZT16.5 (530 to 670 nmol g⁻¹ fresh weight). These values decreased during the dark period, reaching a value of approx. 340 nmol g⁻¹ fresh weight by the end of the night (Figure 4D).

Localization of Ser419 in the C₄-NADP-ME structure

We recently solved the crystal structures of C₄-NADP-ME of maize (ZmC₄-NADP-ME; pdb-code 5OU5) and sorghum (SbC₄-NADP-ME; pdb-code 6C7N) which both display a homotetrameric assembly composed of two dimers (monomers A and B and monomers C and D, respectively (Figure 5A) (Alvarez et al., 2019). The overall structure of SbC₄-NADP-ME is highly similar to that of ZmC₄-NADP-ME (rmsd 0.81 Å over 1584 Cα atoms), although parts of monomer C and D (residues 360 to 530) are not unambiguously traceable in the electron density. However, SbC₄-NADP-ME monomer A and B are of high quality and clearly show a NADP molecule bound in the active site in each monomer (Figures 5A,B and Supplemental Figure 3A).

In order to elucidate the influence of S419 phosphorylation on the biochemical changes observed in C₄-NADP-ME, we analyzed the cofactor binding site on the crystal structure of SbC₄-NADP-ME in a complex with NADP (pdb-code 6C7N; (Alvarez et al., 2019)). The nicotine amide moiety of NADP interacts the O-atoms of S535, whereas both oxygen atoms of the ribose are hydrogen bonded by the N-atoms of N492 and the side chain O of S491. The phosphate O-atoms show several interactions to the side and main chain atoms of E386, A387 and N331, while the ribose 3'-OH-group is hydrogen bonded to the backbone nitrogen of

- A384. Most interactions are present between the 2'-phosphate of the adenosine moiety and
- 300 the protein, i.e. to main and side chain atoms of K435 and S419 (Figure 5C, Supplemental
- Table 2). These analyses clearly demonstrate that S419 plays an important role in NADP
- 302 binding.
- 303 Using the structural information, we also found that Ser419 is located on the solvent-exposed
- 304 surface of the enzyme. It might, therefore, be spatially available for the interaction with a
- 305 kinase/phosphatase (Supplemental Figure 3B,C). Analysis of known kinase/phosphatase
- 306 binding motifs associated with the identified phosphorylation site in ZmC₄-NADP-ME
- 307 indicated the presence of a β-adrenergic receptor kinase (BARK) substrate motif DSKGL
- 308 (Amanchy et al., 2007) (Supplemental Figure 1).

- NADP binding is less favorable to the S419E and phosphorylated variants than to wild
- 311 type ZmC_4 -NADP-ME
- In order to assess differences in the binding affinity of NADP to WT ZmC₄-NADP-ME, the
- variant carrying the phosphomimetic substitution S419E, and the phosphorylated enzyme
- pS419, we performed ten independent molecular dynamics (MD) simulations of 100 ns length
- each on the different complexes. As to the protein systems, only moderate structural changes
- 316 were observed during the MD simulations, in particular in the second halves of the
- 317 trajectories (Supplemental Figure 5). However, preliminary simulation results showed that,
- 318 especially for the variant systems, NADP has the tendency to unbind (Supplemental Figure
- 319 6). This finding already indicates that the affinity of NADP to the S419E and pS419 variants
- 320 is lower than to the WT. Furthermore, the higher mobility of the cofactor in the variant's
- binding site may explain the ~6-fold lower turnover rate (k_{cat}) of the S419E variant compared
- 322 to WT ZmC₄-ME (Figure 2), as then obtaining a reactive configuration with malate becomes
- 323 less likely.
- 324 As the NADP unbinding would compromise the comparability of results of effective binding
- energy calculations (Homeyer et al., 2014), the MD simulations were repeated restraining
- NADP to the respective binding sites (Supplemental Figure 7). Effective binding energies
- were then computed by the MM-PBSA method (Gohlke and Case, 2004; Miller et al.,
- 328 2012; Wang et al., 2016), employing the single-trajectory approach on the second halves of the
- 329 trajectories and considering contributions due to gas-phase energies and solvation free
- energies but neglecting contributions due to changes in the configurational entropy (see
- Methods part for a justification). In line with the preliminary simulation results, the effective

energy of binding of NADP towards the S419E and pS419 variants is significantly larger compared to that of NADP binding to the WT (Figure 6A), indicating that binding to the two variants is much less favorable than to the WT. This finding agrees with the experimental observation that no saturation concentration of NADP could be reached during biochemical characterization of the S419E variant (Figure 2).

Furthermore, a structural decomposition on a per-residue level of the terms contributing to the effective binding energy revealed only minor differences between the variants and the WT in the van der Waals interactions and non-polar contributions of the solvation free energy (Figure 6B). By contrast, the variants' lower binding affinity to NADP is caused by an increase in the electrostatic energy, which is only partially compensated for by a more favorable polar solvation (Figure 6B). These energetic changes coincide on the structural level with a loss of the hydrogen bond between S419 and the 2'-phosphate of NADP in WT and charge repulsion of the negatively charged opposing groups in the variants (Figure 6C).

DISCUSSION

ZmC₄-NADP-ME is phosphorylated in vivo at a serine that is directly involved in NADP

binding

Through mass spectrometry, we identified a single phosphorylation event of ZmC₄-NADP-ME at S419 in maize leaves. Phosphorylation levels increase after the light is turned on, with a peak at ZT2. Through mutational analysis and biochemical characterization of ZmC₄-NADP-ME WT and enzyme variants, we demonstrate that the phosphomimetic mutant S419E has highly reduced affinity to the cofactor NADP as well as lower catalytic activity compared to the non-phosphorylated enzyme. S419E presented a low residual activity at the stromal pH in the light, indicating that a negative charge at this site of ZmC₄-NADP-ME drastically decreases its activity. Analysis of the crystal structures of Zm- and SbC₄-NADP-ME indicated that S419 is located on the surface of the enzyme, which makes it spatially available for the interaction with a kinase/phosphatase. Moreover, analysis of the crystal structure indicates that S419 is directly involved in NADP binding. Molecular dynamics simulations and free energy calculations revealed that the effective energy for NADP binding is less favorable in the phosphomimetic (S419E) and the phosphorylated variants than in the WT. Additionally, the higher mobility of the cofactor in the variants' binding sites likely lead to binding positions of NADP that are not suitable for a reaction with the substrate. This explains the highly reduced affinity of S419E for NADP and suggests that phosphorylation of S419 modulates the activity of ZmC₄-NADP-ME by creating unfavorable binding conditions for its cofactor.

367 Furthermore, we observed conservation of the S419, as well as of a β-adrenergic receptor 368 kinase (BARK) substrate motif (DSKGL), which includes the S419, among plastidic 369 photosynthetic and non-photosynthetic NADP-ME isoforms within the Poaceae 370 (Supplemental Figure 1). This pattern of sequences conservation and the fact that we found 371 that only the C₄-NADP-ME isoform is phosphorylated in leaves suggests that the use of 372 reversible phosphorylation of S419 to control the activity of NADP-ME in photosynthetic 373 tissues appeared with the evolution of the C₄ pathway and should involve a BSC chloroplastic 374 kinase, which might have been co-opted for this specific task.

375

376

377

378

379

380

381

382

383

384

385

386

387

388

389

390

391

392

393

394

395

396

397

Phosphorylation of ZmC₄-NADP-ME at S419 is a mechanism to fine-tune the enzymatic activity

The operation of the C₄ pathway requires a deep synchronization between mesophyll cells and BSCs during a day-night cycle (Bailey et al., 2007). To efficiently concentrate CO₂ in BSC chloroplasts, coordination of C₄-NADP-ME decarboxylation and Rubisco carboxylation rates is imperative as this will prevent loss of the CO₂ released by C₄-NADP-ME. During the night, when the photosynthetic pathway is inactive, C₄-NADP-ME activity is regulated through two processes: on the one hand, the enzyme is allosterically inhibited by malate, on the other hand, it partially loses its active quaternary oligomerization state (Iglesias and Andreo, 1990; Saigo et al., 2004; Saigo et al., 2013; Alvarez et al., 2019). Production of malate in mesophyll cells and its decarboxylation in BSCs must also be coordinated to accommodate the large and rapid flux changes that occur during the day. We show that malate concentrations in total maize leaf extracts tend to decrease during the night and increase after the onset of light, quickly reaching values that are maintained during the whole light period. This profile of malate concentrations in maize leaves is different from that described in some C₃ plants such as *Arabidopsis*, where malate functions as a transient carbon storage molecule; in these C₃ plants, malate concentrations increase continuously during the day and decrease during the night (Fahnenstich et al., 2007; Zell et al., 2010). The differences of malate levels between the end of the night and the day in maize leaves is likely mostly due to the activity of the C₄ concentrating mechanism.

Apart from the contribution of malate decarboxylation, respiration of CO₂ in BSC also contributes to the carbon concentrating mechanism (Bellasio and Griffiths, 2014a;b). It is

possible that under our conditions of growth, at ZT2, respiration in BSC is high enough to make an important contribution to CO₂ fixation by Rubisco. In such conditions, decarboxylation of malate by a fully active C₄-NADP-ME could lead to high CO₂ levels in BSC resulting in increased wasteful leakage of CO₂ to mesophyll cells (Kromdijk et al., 2014). The naturally evolved efficiency of C₄ photosynthesis requires the tight regulation of CO₂ supply to Rubisco within the BSCs in order to minimize leakiness and associated energy costs (Furbank et al., 1990). As a consequence, a decrease in C₄-NADP-ME activity would avoid extra waste of ATP for the operation of the C₄ carbon concentration mechanism. The cooperation of the PEPC-driven carbon concentration and respiration-driven mechanisms require plasticity, as the extent in which each of these mechanisms is involved may depend on changes of environmental conditions. Phosphorylation of ZmC₄-NADP-ME at S419 during the first hours in the light might thus be a mechanism to fine-tune the enzymatic activity, helping to adjust the use of malate in the BSC to avoid CO₂ leakiness and energy waste. The functional importance of this molecular switch is probably linked to environmental changes such as the photosynthetically active radiation, shade by canopy, and water availability environmental conditions. Regulation of C₄-NADP-ME activity via phosphorylation may also be important in the context of biochemical flexibility of the C₄ pathway. Aspartate movement to maize BSCs carries approximately 4% of the CO₂ for the C₃ cycle. Approximately 40% of this C₄-acid is decarboxylated by PEPCK (Arrivault et al., 2017); the remainder aspartate is converted to malate and decarboxylated through NAD(P)-ME. There exists a flexible partitioning of C₄ decarboxylation activity between NADP-ME and PEPCK in response to environmental conditions in maize (Furbank, 2011; Sharwood et al., 2014). In this context, we hypothesize that phosphorylation of ZmC₄-NADP-ME at Ser419 might be a mechanism to rapidly decrease the activity of C₄-NADP-ME and with this to switch the use of malate to aspartate according to the metabolic demands imposed by a constantly changing environment.

398

399

400

401

402

403

404

405

406

407

408

409

410

411

412

413

414

415

416

417

418

419

420

421

422

423

424

425

426

427

428

429

430

A currently highly popular goal within the plant scientific community is the improvement of photosynthesis by introducing the C_4 concentrating mechanism into C_3 plants. Our results are of great importance in this context, as they describe a novel regulation of a C_4 enzyme critical for an efficient C_4 cycle. Further work should be now directed towards elucidating the environmental conditions in which this regulatory mechanism is required, and if it effectively contributes to the coordination of the C_4 and C_3 cycles and hence to the metabolic flexibility of C_4 plants in response to fluctuating environments.

432

433

METHODS

Plant growth conditions

- 434 For the mass spectrometry analysis, Zea mays (B73) seeds were germinated for 48h in the
- 435 dark at 28°C and then transferred to a soil:turf (1:1) mixture. Plants were grown under the
- 436 following conditions: light/dark cycles of 16/8 h at 28°C/26°C; light intensity of 450 µmol m⁻²
- 437 s⁻¹. For metabolite analysis and determination of total NADP-ME enzyme activity, plants were
- 438 grown in Floraton I soil in a Conviron® E15 plant growth chamber under following conditions:

One-third (from leaf tip) of maize leaves (3rd leaf) from 12-day-old seedlings were harvested,

immediately frozen in liquid nitrogen and stored at -80 °C until further analysis. Maize leaves

light/dark cycles of 16/8 h at 25°C/20°C; light intensity of 700 µmol m⁻² s⁻¹. 439

440

441

442

443

Sample preparation for LC-MS analysis

- 444 were collected at ZT (Zeitgeber time) 0.5, 2, 4, 15.5, 16.5, 20, and 23.5; where ZT0 = light on 445 and ZT16 = light off. At each time point, 4 pools of 5 maize leaves were collected. Each pool 446 constitutes one biological replicate. Frozen maize leaves were ground with mortar and pestle 447 in liquid nitrogen until a fine powder was obtained. Protein extraction was performed directly 448 in Lysis Buffer as previously described (Luis et al., 2016). For the total protein analysis, 449 protein extracts were loaded onto 4-12% bis-tris polyacrylamide gels (NuPAGE, 450 ThermoFisher Scientific, Waltham, MA USA) and electrophoresed for a short time (10-15 451 min). The whole bands containing the entire protein extract (2-3 cm long) were excised and 452 in-gel digested with trypsin followed by peptide desalt with C18 tips (Thermo Scientific, 453 Rockford IL USA). For the phosphopeptide analysis of NADP-ME, protein extracts were 454 loaded onto the same kind of gels (4-12% bis-tris polyacrylamide gels, NuPAGE,
- 455 ThermoFisher Scientific, Waltham, MA USA), electrophoresed at a constant voltage of 25V
- 456 for 10 min and then for 150V until the Bromophenol Blue reached the bottom of the gel.
- 457 Then, the gel fractions containing the NADP-ME (ranging from just below the 63 kDa to just
- 458 after the 75 kDa) were excised, in-gel digested with trypsin and further lyophilized to dryness.
- 459 Vacuum dried peptides were first desalted using C18 tips (Thermo Scientific, Rockford IL
- 460 USA) before being subjected to phosphopeptide enrichment using TiO₂ beads (TiO₂ Mag
- 461 Sepharose, GE Healthcare, Uppsala, Sweden) according to manufacturer's instructions.

LC-MS using an AB Sciex TripleTOF 6600

463

464

465 MA USA), coupled to a nanoLC Eksigent 425 system (AB Sciex, Framingham, MA USA). 466 RP-HPLC was performed in a trap and elution configuration using a nano cHiPLC trap column (Eksigent ChromXP C18-CL, 3 µm particle size, 120 Å pore size, 0.5 mm x 200 µm 467 468 I.D., AB Sciex, Framingham, MA USA) and an analytical column (Eksigent ChromXP C18-469 CL, 3 µm particle size, 120 Å pore size, 15 cm × 75 µm I.D., AB Sciex, Framingham, MA 470 USA). Samples were loaded into the trap column at a flow rate of 2 µL min⁻¹ for 10 min using 471 100% solvent A (0.1% formic acid in water) and eluted at a flow rate of 300 nL/min using a 472 stepwise gradient: 0-1min, 4.5% B (0.1% formic acid in acetonitrile); 1-91min, 29.7% B; 91-473 93, 79.2% B; 93-108min, 79.2% B; 108-110min, 4.5% B; 110-127min, 4.5% B. Samples 474 were run in information-dependent acquisition (IDA) mode to perform peptide and protein identification in order to generate a spectral library for the SWATH quantification. This 475 476 spectral library was created by combining all the IDA.wiff files in unison using ProteinPilot 477 5.0 (AB Sciex). Database search was performed using the Paragon algorithm, which is 478 embedded in ProteinPilot software, v. 5.0 (AB Sciex, Framingham, MA USA). A Paragon 479 search method was created with the following settings: sample type, identification; cys 480 alkylation, acrylamide; digestion, trypsin; instrument, tripleTOF 6600; special factors, 481 phosphorylation emphasis and gel-based ID; species, none; ID focus, biological 482 modifications; search effort, thorough; detected protein threshold, >0.05. The searches were 483 conducted using a UniProt database containing all reviewed protein sequences for the species 484 Zea mays. A false discovery rate threshold was set to below 1%. 485 As for the SWATH-MS analysis, four replicates from each one of the seven time points 486 collected were analyzed by LC-MS using the setup described for the IDA runs. SWATH-MS 487 data were acquired with a standard SWATH acquisition method, using a set of 32 overlapping 488 SWATH windows covering the precursor mass range of 400-1200 m/z. For each SWATH 489 window, the Q1 transmission width was 26 m/z (containing 1 m/z for the window overlap). 490 At the beginning of each cycle, a 50 ms survey scan (350-1250 m/z) was acquired for 491 instrument calibration, and the subsequent SWATH windows were collected from 100 to 492 1800 m/z for 60 ms, resulting in a cycle time of 2.02 s. Data processing was performed using 493 SWATH processing plug-in for PeakView 2.2 (AB Sciex, Framingham, MA USA). Briefly, 494 peptides were confirmed by finding and scoring peak groups, which are a set of fragment ions 495 for the peptide. Target fragment ions, up to 5, were automatically selected as previously 496 described (Lambert et al., 2013) criteria: (i) fragment ions for a selected peptide were ranked

Samples were analyzed using a TripleTOF 6600 mass spectrometer (AB Sciex, Framingham,

according to ion intensity; (ii) ions higher in m/z than the y4 fragment ion for each selected peptide were ranked highest; (iii) ions within the SWATH isolation window were excluded from selection; (iv) if insufficient target ions were found, ions lower than y4 but outside of the SWATH window were chosen; (v) if there were still insufficient ions, then fragment ions from within the SWATH window region were chosen. Peak group confidence threshold was determined based on an FDR analysis using the target-decoy approach, and 1% extraction FDR threshold was used for all the analyses. Peptides that met the 1% FDR threshold in all the four replicates were retained, and the peak areas of the target fragment ions of those peptides were extracted across the experiments using an extracted-ion chromatogram window of 12 min. ZmC₄-NADP-ME protein levels were estimated by summing the areas of all the transitions from all the peptides for a given protein and normalized to the total area (Collins et al., 2013). As for the ZmC₄-NADP-ME phosphopeptide (acVWLVDpSK) levels, they were estimated by summing the areas of the transitions obtained for this phosphopeptide and normalized to the sum of the area of all the transitions from all the peptides within the same region (that include S419) for each of the time points.

512

513

497

498

499

500

501

502

503

504

505

506

507

508

509

510

511

Site-directed mutagenesis of ZmC₄-NADP-ME

- As template for the PCR reaction (first step of the site-directed mutagenesis), pET32::WT NADP-ME expression construct (Detarsio et al., 2003) was used. Point mutations were
- 516 introduced into the protein-coding region by performing site-directed mutagenesis with the
- 517 following "back-to-back" primers: 5'-TCGTCCACCAGCCAAAC-3' and
- 518 5'-AAAGGGTTTGATTGTTGACTCTCG-3' ("for" and "rev" primers for the introduction of
- the S419E mutation; resulting construct has been termed pET32a::S419E NADP-ME) and
- 520 5'-GCGTCCACCAGCCAAACC-3' as the "for" primer and the same "rev" primer as used in
- 521 case of the first mutagenesis for the introduction of the S419A mutation (resulting construct
- 522 has been termed pET32a::S419A-NADP-ME). All primers used for the mutagenesis
- 523 procedure were phosphorylated at the 5'-terminus.
- 524 Site-directed mutagenesis has been performed as follows: usually, 5 similar 50 μL PCR
- reactions were performed simultaneously. Obtained DNA was pulled together and (after
- digestion from the agarose gel, if needed) subjected to the self-ligation by using the T4 DNA
- 527 ligase (ThermoFisher Scientific). Self-ligation was performed by incubation of the mix at 22
- °C for 1 h. Subsequently, inactivation of the ligase by incubation of reaction mix at 65 °C for
- 529 10 min has been performed. In order to destroy the methylated WT (sample) DNA, the

reaction mix after self-ligation has been subjected to the digestion at 37°C for 2 h by the DpnI (Thermo Scientific). After digestion, the DpnI has been inactivated by incubation at 80°C for 5 min. Concluding, obtained constructs were used for the transformation of the chemically-competent *E. coli* DH5α cells. After plasmid preparation, the success of the site-directed mutagenesis procedure has been confirmed by sequencing with three primers covering the whole length of the protein-coding region.

536

537

538

539

540

541

542

543

544

545

546

547

548

549

550

551

552

553

554

555

556

557

558

559

560

561

530

531

532

533

534

535

Expression and purification of recombinant ZmC₄-NADP-ME

The WT and two obtained mutated pET32::ME constructs were used for the transformation of the E. coli strain Rosetta (DE3) (Novagen). For the heterologous protein production, transformed cells were grown in 400 mL LB medium at 37 °C and agitation of 110 rpm in the presence of 100 µg mL⁻¹ ampicillin and 34 µg mL⁻¹ chloramphenicol until an OD₆₀₀ of 0.6 -0.8 was reached. To induce protein expression, final concentration of 1 mM isopropyl-β-Dthiogalactopyranoside (IPTG) was added to the culture and cells were grown for additional 20h under the same conditions. Harvest of the cells was performed by centrifugation at 4,000 g for 15 min. Obtained pellets were transferred into 50 mL Falcon tubes and were stored at -20°C until further usage. For the protein extraction, pellets were thawed on ice and resuspended in 20 mM Tris-HCl (pH 8.0) containing 500 mM NaCl, 5 mM imidazole, 2 mM phenylmethanesulfonyl fluoride (PMSF) and a spatula-tip amount of lysozyme, sonicated and centrifuged at 14,000 g for 20 min at 4°C to remove cell debris. Obtained supernatant has been deployed for protein purification using gravity-flow immobilized metal ion chromatography on nickel-nitrilotriacetic acid agarose (Ni-NTA Agarose, Qiagen). Prior to the supernatant loading, the column was equilibrated with 20 mM Tris-HCl buffer containing 500 mM NaCl and 5 mM imidazole. After the supernatant was loaded, columns were washed in four steps with 20 mM Tris-HCl (pH 8.0) and 500 mM NaCl buffers containing increasing concentrations of imidazole (5, 30, 40 and 50 mM) in order to isolate the His-tagged NADP-MEs. Elution was performed using four times 500 µL of 20 mM Tris-HCl buffer containing 500 mM NaCl and 300 mM imidazole. Eluted protein from the first elution fraction has been used for further kinetic measurements.

For all constructs used in this work, the calculated molecular mass of the expressed protein corresponded to the expected molecular mass of the fusion protein as follows: mature ZmC₄-NADP-ME (63.4 kDa) plus 17.3 kDa encoded by the expression vector.

Protein quantification, gel electrophoresis and immunological detection

Protein concentration was determined using the PierceTM BCA Protein Assay Kit (Thermo 564 565 Fischer Scientific). SDS-PAGE was performed using 12% (w/v) polyacrylamide gels 566 according to Laemmli (Laemmli, 1970). Proteins were visualized by staining with Coomassie 567 Brilliant Blue or electroblotted onto a nitrocellulose membrane (Thermo Scientific) for 568 immunological detection. The membranes were incubated for at least 1 h with the 1:7500 569 dilution of Anti-His-Tag antibody coupled to horseradish peroxidase (Anti-His-HRP; Miltenyi Biotec). After several washing step the membranes were incubated with a 1:2500 570 571 dilution of the Goat Anti-Rabbit IgG Antibody HRP-conjugate (Merck). The chemiluminescence signal was detected with ImmobilonTM Western Chemiluminescent HRP 572 Substrate (Merck Millipore) with subsequent visualization on an LAS-4000 Mini 573 574 Luminescent Image Analyzer (GE Healthcare Life Sciences formerly Fuji).

575

576

577

578

579

580

581

582

583

584

585

586

587

588

589

590

591

592

593

594

563

Determination of kinetic parameters

NADP-ME activity was determined using a Synergy HT Biotek® Plate Reader system by measuring the formation of NADPH at 340 nm (extinction coefficient = 6.22 mM⁻¹ cm⁻¹) at room temperature. The standard assay medium contained 0.5 mM NADP⁺, 10 mM MgCl₂, 4 mM L-malate, 50 mM Tris-HCl (pH 8.0) and 0.1 - 0.8 µg enzyme per well in a final volume of 200 µL. The dependence of the activity with the pH of the medium was determined with the standard assay medium using different buffer systems: 50 mM MES (pH 5.5-6.5), 50 mM Tricine-Mops (pH 7.0-7.5), and 50 mM Tris-HCl (pH 7.5-9.0). The Michaelis ($K_{\rm m}$ in case of WT and S419A) and apparent Michaelis (K_{mapp} in case of S419E) constant of the substrate were determined by varying the concentration of one substrate while keeping the other components constant at fixed concentrations as described for the standard assay medium. NADP concentrations were varied between 2 and 150 µM in case of WT, between 10 and 800 µM in case of S419A and between 10 and 5 mM in case of S419E. Malate concentrations were varied between 0.001 and 8 mM in case of WT and S419A and between 0.1 and 10 mM in case of the S419E. As S419 was not saturated with NADP at least until 5 mM NADP, the $K_{\rm m}$ NADP for S419E could not be estimated. Measuremets of enzymatic activity using high NADP concentrations are technically impair by the high absortion of this compound; thus, other kinetic parameters of S419E, apparent parameters (k_{catapp} and K_{mapp} malate) were estimated using 0.5 mM NADP. All kinetic parameters were calculated using at least three biological replicates and adjusted to non-lineal regression. Data were fitted with the Prism 6 (GraphPad Software).

Circular Dichroism

- All recombinant versions of ZmC₄-NADP-ME were subjected to circular dichroism (CD) analysis in 20 mM NaP_i, pH 8.0 or 7.0; 5 mM MgCl₂. Protein concentration was determined at 280 nm using a Jasco V-650 spectrophotometer. The protein concentration (c, g L⁻¹) was calculated by the equation $c = A_{280} \cdot Mw/(\varepsilon \cdot d)$, in which ε represents the molar extinction coefficient at 280 nm (76250 L mol⁻¹ cm⁻¹), d is the cell path (1 cm) and Mw is molecular weight (80.7 kDa for all three proteins).
 - CD spectra between 240 and 190 nm were obtained averaging 10 repetitive scans in a Jasco J-810 spectropolarimeter. Mean residue ellipticity ($[\Theta]$, deg cm² dmol⁻¹) was obtained by the equation $[\Theta] = MRW \cdot \Theta/(10 \cdot c \cdot d)$, where MRW (the mean amino acid residue weight) was calculated as relation of the protein's molecular weight (Mw) to the number of peptide bonds (N-1; where N is the number of amino acids in the chain), d is the cell path (0.1 cm), c is the protein concentration and Θ is the observed ellipticity in millidegrees (machine units). Determination of the protein secondary structure contents was performed using the CONTIN-LL method (van Stokkum et al., 1990) and the reference dataset 4 (Sreerama and Woody, 2000) at the Dichroweb online server (http://dichroweb.cryst.bbk.ac.uk) (Whitmore and Wallace). Prism Software (http://www.graphpad.com/scientific-software/prism/) was used for

Analytical Ultracentrifugation

visualization of the deconvolution by Dichroweb.

Sedimentation velocity experiments were carried out using a Beckman Optima XL-A Analytical Ultracentrifuge. All recombinant versions of ZmC₄-NADP-ME were assayed in 10 mM Tris-HCl buffer (pH 7.0 and 8.0) with addition of 5 mM MgCl₂. Buffer exchange procedure was performed using the Amicon Ultra 0.5 mL centrifugal units with nominal molecular weight limit of 50 kDa (Merck) and final protein concentration was adjusted to 0.6 mg mL⁻¹. Samples (230 μg) and corresponding buffer solutions (400μL) were loaded into aluminium double sector centerpieces separately and built up in a Beckman An-50 Ti rotor. Experiments were performed at 20 °C and a rotor speed of 35,000 rpm. Protein samples were monitored by UV absorbance at 280 nm in a continuous mode with a radial resolution of

0.003 cm. In time intervals of about 2 min scans of the radial concentration profile were collected until the protein was fully sedimented. Data were analysed using the c(s) model in the software package SEDFIT (Schuck and Rossmanith, 2000). For data analysis, a resolution of 0.1 S with a confidence level (F-ratio) of 0.95 was chosen for the appropriate *s*-value range within 0 to 30.0 S. Density and viscosity of the solvent had been calculated with the software Sednterp from tabulated values; $\rho = 0.99885$ g cm⁻³ and $\eta = 0.01006$ g cm⁻¹s⁻¹. The protein partial specific volume \bar{v} applied for WT and mutants was 0.7387 cm³ g⁻¹. Sedimentation coefficients are reported as $s_{20, w}$ values, i.e. normalized to 20°C and water as a solvent. Graphic output was generated by Gussi (Version 1.2.1) (Brautigam, 2015) and the final sedimentation coefficient distribution was normalized based on the maximum peak height.

637

638

627

628

629

630

631

632

633

634

635

636

NADP-ME activity measurements in extracts of maize leaves

639 Maize leaves were collected at ZT (Zeitgeber time) 0.5, 2, 4, 8, 15.5, 16.5, 20 and 23.5; where ZT0 = light on and ZT16 = light off. One-third (from leaf tip) of maize leaves (3rd and 4th 640 641 leaf) from 12-day-old seedlings were harvested, immediately frozen in liquid nitrogen and 642 stored at -80 °C until further analysis. Soluble protein extracts were prepared by 643 homogenizing 0.25 g of frozen maize leaves in 500 µL of ice-cold extraction buffer 644 containing 100 mM Tris-HCl (pH 8.0), 5 mM MgCl₂, 0.1 mM EDTA, 10% (v/v) glycerol, 645 2 mM DTT, 1 mM PMSF. The homogenate was clarified by centrifugation at 20,000 g during 646 20 min at 4°C. Protein concentration of the protein extract was determined using the Amido 647 Black assay (Schaffner and Weissmann, 1973). NADP-ME activity was measured in medium containing 50 mM Tris-HCl (pH 8.0), 10 mM MgCl₂, 0.5 mM NADP, 10 mM L-malate and 648 649 1.5 - 2.2 µg protein extract in a final volume of 0.2 mL. The reaction was started by addition of NADP⁺. Measurements were conducted using three independent replicates. 650

651

652

Gas Chromatography - Mass Spectrometry (GC-MS) analysis

- Frozen maize leaves were ground in liquid nitrogen until a fine powder was obtained. Ground
- material (around 50 mg) was extracted in methanol:chloroform:water (5:2:2) with ribitol for
- internal standardization as described by Lee and Fiehn (Lee and Fiehn, 2008).
- 656 An aliquot of the supernatant (150 μl) was dried under vacuum, and the residue was
- derivatized for 120 min at 37°C (in 60 µl of 30 mg ml⁻¹ methoxyamine hydrochloride in
- pyridine) followed by a 30 min treatment at 37°C with 120 µl of MSTFA. The GC-MS

system used was a gas chromatograph coupled to a time-of-flight mass spectrometer (Leco Pegasus HT TOF-MS). An auto sampler Gerstel Multi-Purpose system injected the samples. Helium was used as carrier gas at a constant flow rate of 2 mL s⁻¹ and gas chromatography was performed on a 30 m DB-35 column. The injection temperature was 230°C and the transfer line and ion source were set to 250°C. The initial temperature of the oven (85°C) increased at a rate of 15°C/min up to a final temperature of 360°C. After a solvent delay of 180 s mass spectra were recorded at 20 scans s-1 with m/z 70-600 scanning range. Chromatograms and mass spectra were evaluated by using Chroma TOF 4.5 (Leco) and TagFinder 4.2 software (Ishizaki et al., 2005;Lisec et al., 2006).

Generation of the complex structures

For the complex preparation we used the monomeric *apo* structure of ZmC₄-NADP-ME (aa 132-628, PDB ID 5OU5). Based on the structural alignment with ME from pigeon liver (PDB ID 1GQ2) and SbC₄-NADP-ME (PDB ID 6C7N), a Mg²⁺ ion and NADP were placed into the active site of ZmC₄-ME. Subsequently, the complex was protonated using the Structure Preparation Tool and Protonate3D implemented in MOE (2019) at pH 8.0. The structures of the enzyme carrying a substitution or the phosphorylated residue were generated by replacing S419 either by glutamate or phosphoserine in LEaP (Case et al., 2005).

Molecular dynamics simulations of NADP/ZmME complexes

679 System setup

The following procedures were performed using the Amber18 software package (Case et al., 2018). We used tLEaP to solvate each of the complexes in a periodic box of TIP3P water (Jorgensen et al., 1983), in such a way that the distance between the edges of the box and a solute atom is at least 11 Å. The system was charge-neutralized by replacing random water molecules by sodium ions. The ff14SB force field (Hornak et al., 2006) was used for parameterizing the protein, and Mg²⁺ parameters were taken from the 12-6 LJ set of ion parameters by Li and Merz (Li et al., 2013). The phosphoserine parameters were taken from phosaa10 (Homeyer et al., 2006;Steinbrecher et al., 2012) and modified to be compatible with ff14SB. Partial charges according to the RESP procedure (Bayly et al., 1993) for NADP were derived from the R.E.DD.B. (Dupradeau et al., 2008) project F-91, while for bond parameters the GAFF force field (Wang et al., 2004) was used. In order to remove initial clashes due to

- the introduction of the larger side chains replacing S419, for the modified systems an energy
- 692 minimization of this residue was performed with pmemd (Le Grand et al., 2013; Case et al.,
- 693 2018) prior to the thermalization.
- 694 Thermalization
- All simulations were carried out using the GPU version of pmemd. The Langevin thermostat
- 696 (Pastor et al., 1988) was used for temperature control with a collision frequency of $\gamma = 2.0 \text{ ps}^{-1}$
- 697 ¹. For treatment of long-range electrostatic interactions the Particle Mesh Ewald method
- 698 (Berendsen et al., 1984) was used with a cutoff of 8.0 Å. The SHAKE algorithm (Ryckaert et
- al., 1977) was used to constrain bond lengths involving hydrogen atoms, and hydrogen mass
- repartitioning (Hopkins et al., 2015) was used to allow for simulation steps of 4 fs.
- 701 Initially, an energy minimization was performed independently on solvent and solute atoms
- for 3,000 steps each with the steepest decent algorithm, followed by 2,000 steps with the
- 703 conjugate gradient algorithm. Thereafter, all atoms were energy-minimized the same way.
- Then, the systems were heated to 300 K at a constant heating rate over 20 ps of NVT-MD and
- simulated for further 5 ps at 300 K. For density adaptation, 75 ps of NPT-MD were performed
- with a pressure relaxation time of $\tau_p = 1.0$ ps, followed by 1,700 ps of NPT-MD with the same
- 707 restraints and $\tau_p = 2.0$ ps. For all these steps, positional restraints of 2.0 kcal·mol⁻¹·Å⁻² were
- 708 applied to the enzyme's C_{α} -atoms and NADP. Ten further iterations of minimization were
- performed on the system with iteratively decreasing restraints on the solute atoms (force
- 710 constants ranging from 2 to 0 kcal·mol⁻¹·Å⁻²), with 500 steps of steepest decent minimization
- and 500 steps of conjugate gradient minimization each. Finally, the systems were heated
- again to 300 K over 100 ps of NVT-MD, followed by 3,100 ps NVT-MD. Again, positional
- restraints with a force constant of 2.0 kcal·mol⁻¹·Å⁻² were applied to the enzyme's C_{α} -atoms
- and NADP.
- 715 Production
- For each of the three systems ten individual NVT-MD simulations of 100 ns length were
- performed. Since especially in the mutated systems the binding pose of NADP was not stable,
- and large conformational rearrangements would compromise the effective binding energy
- 719 calculations, we restrained NADP within the binding site in all three systems by a distance
- restraint between the C_{α} of S435 and the nicotinamide of NADP using a one-sided harmonic
- potential with a force constant of 2.0 kcal·mol⁻¹·Å⁻². Coordinates for post-processing and
- further analysis were extracted every 100 ps. For geometric analyses, CPPTRAJ (Roe and
- 723 Cheatham, 2013) was used.

- 724 Calculation of effective binding energies
- 725 The calculation was performed using MMPBSA.py from AmberTools18 (Miller et al.,
- 726 2012; Case et al., 2018). For all systems the change of the effective energy due to binding of
- NADP was calculated using the single-trajectory MM-PBSA approach on the last 50 ns of
- trajectory (Gohlke and Case, 2004; Wang et al., 2016). All counter ions and water molecules
- were stripped from the trajectory, and the sum of electrostatic and van der Waals energies was
- calculated for each snapshot using the above-mentioned force fields (internal energies cancel
- in this approach). The polar part of the solvation free energy was calculated at the level of
- Poisson-Boltzmann theory, with the dielectric constants set to 80 for the solvent and 4 for the
- solute and an ionic strength of 300 mM. The nonpolar part of the solvation free energy was
- calculated by separating the attractive and repulsive terms, as shown by Tan *et al.* (Tan et al.,
- 735 2007), using as a surface tension 0.0378 kcal mol⁻¹ Å⁻². Previous studies have shown that
- 736 inclusion of configurational entropy is crucial for calculating *absolute* binding free energies
- 737 (Hou et al., 2011; Genheden and Ryde, 2015; Ben-Shalom et al., 2017). In the present study,
- however, we were interested in *relative* binding free energies and, thus, decided to neglect
- contributions due to changes in the configurational entropy of the ligand or the receptor upon
- complex formation in order to avoid introducing additional uncertainty in the computations
- 741 (Gohlke and Case, 2004; Weis et al., 2006; Hou et al., 2011).

- 743 **SUPPLEMENTAL DATA**
- Supplemental Figure 1. Alignment of plastidic C₄- and nonC₄-NADP-ME sequences in
- Poaceae showing conservation of S419 and the BARK substrate motif (DSKGL).

746

- 747 Supplemental Figure 2. SDS-PAGE stained with Coomassie-Blue (lines 1-4) and
- analysed by immunoblot (line 5) of protein fractions during the isolation of recombinant
- 749 **ZmC₄-NADP-ME** variants.

750

- 751 Supplemental Figure 3. Representation of the bound cofactor NADP in SbC₄-NADP-ME
- 752 **chain B.**

753

- 754 Supplemental Figure 4. Comparison of the CD spectra of ZmC₄-NADP-ME WT
- 755 **obtained at pH 7.0 and 8.0.**

Supplemental Figure 5. Root mean square deviations of the enzyme's C_a atoms.

758

- 759 Supplemental Figure 6. Root mean square deviations of NADP in the binding site of
- 760 **ZmC₄-NADP-ME**.

761

- Supplemental Figure 7. Root mean square deviations of NADP in the binding site of
- 763 ZmC₄-NADP-ME after restraining NADP to the respective binding sites.

764

- Supplemental Table 1. Secondary structure contents of ZmC₄-NADP-ME WT, S419A
- and S419E estimated from the CD-spectra obtained at pH of 7.0 and 8.0.

767

- Supplemental Table 2. Polar interactions/hydrogen bonds between monomer A of SbC₄-
- NADP-ME and the cofactor NADP with their distances.

770

- 771 Supplemental Table 3. P-values for figure 4.
- 772 **ACKNOWLEDGEMENTS**
- 773 This work was funded by grants of the European Commission (3to4; 289582) to VGM and
- IAA and by the Deutsche Forschungsgemeinschaft (DFG, German Research Foundation)
- under Germany's Excellence Strategy EXC 2048/1 Project ID: 390686111 and EXC 1028
- to VGM. AB acknowledge the support of the iGrad Plant International Graduate Program of
- 777 the HHU for funding. The Center for Structural Studies is funded by the Deutsche
- 778 Forschungsgemeinschaft (DFG Grant number 417919780; INST 208/740-1 FUGG). IAA
- acknowledges FCT Investigator programme and GREEN-it (UID/Multi/04551/2013) for
- funding. SA and ARF acknowledge the support of the German Federal Ministry of Research
- and Education grant Full throttle (BMBF, grant 031B0205A). BMA is a recipient of FCT
- 782 post-doctorate fellowship (SFRH/BPD/98619/2013) and IML is a recipient of FCT doctorate
- 783 fellowship (PD/BD/113982/2015 within MolBioS PD/00133/2012). LC-MS/MS analyses
- were performed at the Mass Spectrometry Unit (UniMS) facility of iBET/ITQB-UNL, Oeiras,
- Portugal. We are grateful for computational support by the "Zentrum für Informations und
- Medientechnologie" at the Heinrich Heine University and the computing time provided by the
- John von Neumann Institute for Computing (NIC) to H.G. on the supercomputer JURECA at
- Jülich Supercomputing Centre (JSC) (user ID: HKF7).

790 **AUTHOR CONTRIBUTIONS**

- 791 Conceptualization, V.G.M.; Methodology, V.G.M. and I.A.A.; Investigation, A.B., B.M.A.,
- 792 A.H., C.E.A., I.M.L., C.D., S.A., D.B., H.G.; Writing Original Draft, V.G.M., I.A.A., A.B.,
- 793 A.H., C.E.A., M.F.D., L.N-S., D.B., H.G.; Funding Acquisition, V.G.M. and I.A.A.;
- Resources, V.G.M., I.A.A., M.F.D, A.F; Supervision, V.G.M., I.A.A., M.F.D.

795

FIGURE LEGENDS

796 797

- 798 Figure 1. TripleTOF 6600 tandem MS data of the phosphopeptide acVWLVDpSK of
- 799 **ZmC₄-NADP-ME.** The detected b (N-terminal, in red) and y (C-terminal, in blue) fragment
- 800 ions are labeled in the spectrum. Ac denotes N-terminus acetylation and pS denotes
- phosphorylated serine. Precursor charge: +2; monoisotopic m/z: 484.7265 Da (-1.60 mmu/-
- 802 3.30 ppm). Confidence (ProteinPilot): 96.4% (Confidence threshold for FDR≤1% was equal
- 803 to 93.7%).

804

- Figure 2. Biochemical characterization of recombinant ZmC₄-NADP-ME versions. A,
- Dependence of the activity, measured using 0.5 mM NADP and 4 mM malate, on the pH of
- the assay. The values represent the mean \pm standard error of at least four independent enzyme
- preparations, each measured in triplicate. **B**, Kinetic parameters at pH 8.0. Kinetic data were
- best fitted by nonlinear regression analysis. The values represent the mean \pm standard error of
- at least three independent enzyme preparations, each measured in triplicate.

811

- 812 Figure 3. Exploration of the secondary structure organization and quaternary
- composition of recombinant ZmC₄-NADP-ME versions. A and B, CD spectra of ZmC₄-
- NADP-ME WT and the two mutated versions obtained at pH 7.0 (A) and 8.0 (B). Ten
- accumulations each were collected from 190 to 260 nm for 0.16 mg mL⁻¹ enzyme, at 20°C.
- 816 Each graph is showing the reconstructed curves obtained by applying CONTIN/LL algorithm
- for data evaluation as provided by the Dichroweb server. **C** and **D**, Continuous sedimentation
- coefficient distribution of ZmC₄-NADP-ME WT and the mutated versions at pH 7.0 (C) and
- 8.0 (D). Data was fitted with the ls-g*(s) model in the software package SEDFIT.

- 821 Figure 4. Measurements of different parameters in extracts of maize leaves during a
- 822 diurnal cycle. A, Quantification of total ZmC₄-NADP-ME protein by SWATH-MS. B,
- Quantification of the phosphopeptide VWLVDpSK, corresponding to the phosphorylation of

ZmC₄-NADP-ME at S419. **C**, Total NADP-ME activity measured with 1.5 - 2.0 μg protein extracts. **D**, Malate concentration assayed by GC-MS analysis. Values represent mean ± standard error of four (A and B) or three (C and D) biological replicates. The dark period is highlighted in grey. Statistical analyses were performed against the first time point in the night (ZT16.5). Letters indicate that the value is significantly different form the reference value evaluated by two-tailed t-test at a, 0.05; b, 0.01; c, 0.001 levels (the precise p-values are shown in Supplementary Table 3). ZT, Zeitgeber Time.

Figure 5. SbC₄-NADP-ME crystal structure and amino acids involved in cofactor binding. **A**, Cartoon and ribbon representation of SbC₄-NADP-ME. Monomer A (red) and B (blue) with bound cofactor NADP (colored sticks). Large parts of chain C and D are not well resolved by electron density; therefore, we depicted these chains as gray ribbons only to clarify the tetrameric assembly. **B**, Monomer A from SbC₄-NADP-ME as surface representation with the bound cofactor NADP (represented by sticks). **C**, Residues involved in cofactor binding are depicted as sticks with labels (distances are omitted for clarity and are listed in Table S2).

Figure 6: Effective free energies of binding of NADP. A, Effective binding energies computed according to the MM-PBSA approach for WT ZmC₄-NADP-ME, the phosphomimetic variant (S419E), and the phosphorylated enzyme (pS419). The error bars indicate the standard error of the mean over 10 individual trajectories. Statistical significance was calculated according to Student's *t*-test. **B**, The contribution of the different energy terms, computed as variant's energy term minus the respective energy term of the WT enzyme ($\Delta\Delta G_{\rm eff} = \Delta G_{\rm eff}({\rm Var}) - \Delta G_{\rm eff}({\rm WT})$). Positive terms indicate more favorable binding to the WT enzyme, negative ones to the variant. The error bars show the standard error of the mean of the differences in the individual terms over the trajectories. **C**, Molecular representation of NADP bound to the WT ZmC₄-NADP-ME, the phosphomimetic variant (S419E), and the phosphorylated enzyme (pS419). Interactions with residue 419 are highlighted, showing hydrogen bonds for the WT enzyme with green dashed lines, and charge-charge repulsion for the phosphomimetic and phosphorylated variants with red dashed lines.

REFERENCES

(2019). "Molecular Operating Environment (MOE)". 2019.01 ed.: Chemical Computing Group ULC, 1010 Sherbooke St. West, Suite #910, Montreal, QC, Canada, H3A 2R7).

- Agarie, S., Kai, M., Takatsuji, H., and Ueno, O. (1997). Expression of C3 and C4
 photosynthetic characteristics in the amphibious plant Eleocharis vivipara: structure
 and analysis of the expression of isogenes for pyruvate, orthophosphate dikinase.

 Plant Mol Biol 34, 363-369.
- Alvarez, C.E., Bovdilova, A., Höppner, A., Wolff, C.-C., Saigo, M., Trajtenberg, F., Zhang,
 T., Buschiazzo, A., Nagel-Steger, L., Drincovich, M.F., Lercher, M.J., and Maurino,
 V.G. (2019). Molecular adaptations of NADP-malic enzyme for its function in C4
 photosynthesis in grasses. *Nature Plants* (in press).
 - Alvarez, C.E., Detarsio, E., Moreno, S., Andreo, C.S., and Drincovich, M.F. (2012). Functional characterization of residues involved in redox modulation of maize photosynthetic NADP-malic enzyme activity. *Plant Cell Physiol* 53, 1144-1153.

- Alvarez, C.E., Saigo, M., Margarit, E., Andreo, C.S., and Drincovich, M.F. (2013). Kinetics and functional diversity among the five members of the NADP-malic enzyme family from Zea mays, a C4 species. *Photosynth Res* 115, 65-80.
- Amanchy, R., Periaswamy, B., Mathivanan, S., Reddy, R., Tattikota, S.G., and Pandey, A. (2007). A curated compendium of phosphorylation motifs. *Nat Biotechnol* 25, 285-286.
- Arrivault, S., Obata, T., Szecowka, M., Mengin, V., Guenther, M., Hoehne, M., Fernie, A.R., and Stitt, M. (2017). Metabolite pools and carbon flow during C4 photosynthesis in maize: 13CO2 labeling kinetics and cell type fractionation. *J Exp Bot* 68, 283-298.
- Astley, H.M., Parsley, K., Aubry, S., Chastain, C.J., Burnell, J.N., Webb, M.E., and Hibberd, J.M. (2011). The pyruvate, orthophosphate dikinase regulatory proteins of Arabidopsis are both bifunctional and interact with the catalytic and nucleotide-binding domains of pyruvate, orthophosphate dikinase. *Plant J* 68, 1070-1080.
- Bailey, K.J., Gray, J.E., Walker, R.P., and Leegood, R.C. (2007). Coordinate regulation of phosphoenolpyruvate carboxylase and phosphoenolpyruvate carboxykinase by light and CO2 during C4 photosynthesis. *Plant Physiol* 144, 479-486.
- Bayly, C.I., Cieplak, P., Cornell, W., and Kollman, P.A. (1993). A well-behaved electrostatic potential based method using charge restraints for deriving atomic charges: the RESP model. *The Journal of Physical Chemistry* 97, 10269-10280.
- Bellasio, C., and Griffiths, H. (2014a). Acclimation to low light by C4 maize: implications for bundle sheath leakiness. *Plant Cell Environ* 37, 1046-1058.
- Bellasio, C., and Griffiths, H. (2014b). The operation of two decarboxylases, transamination, and partitioning of C4 metabolic processes between mesophyll and bundle sheath cells allows light capture to be balanced for the maize C4 pathway. *Plant Physiol* 164, 466-480.
- Ben-Shalom, I.Y., Pfeiffer-Marek, S., Baringhaus, K.H., and Gohlke, H. (2017). Efficient Approximation of Ligand Rotational and Translational Entropy Changes upon Binding for Use in MM-PBSA Calculations. *Journal of Chemical Information and Modeling* 57, 170-189.
- Berendsen, H.J.C., Postma, J.P.M., Van Gunsteren, W.F., Dinola, A., and Haak, J.R. (1984).
 Molecular dynamics with coupling to an external bath. *The Journal of Chemical Physics* 81, 3684-3690.
- Boxall, S.F., Dever, L.V., Knerova, J., Gould, P.D., and Hartwell, J. (2017). Phosphorylation
 of Phosphoenolpyruvate Carboxylase Is Essential for Maximal and Sustained Dark
 CO2 Fixation and Core Circadian Clock Operation in the Obligate Crassulacean Acid
 Metabolism Species Kalanchoe fedtschenkoi. *Plant Cell* 29, 2519-2536.
- 906 Brautigam, C.A. (2015). Calculations and Publication-Quality Illustrations for Analytical Ultracentrifugation Data. *Methods Enzymol* 562, 109-133.

- 908 Burnell, J.N. (2010). Cloning and characterization of Escherichia coli DUF299: a bifunctional ADP-dependent kinase--Pi-dependent pyrophosphorylase from bacteria. *BMC* 910 *Biochem* 11, 1.
- 911 Burnell, J.N., and Chastain, C.J. (2006). Cloning and expression of maize-leaf pyruvate, Pi 912 dikinase regulatory protein gene. *Biochem Biophys Res Commun* 345, 675-680.
- 913 Burnell, J.N., and Hatch, M.D. (1985). Regulation of C4 photosynthesis: purification and 914 properties of the protein catalyzing ADP-mediated inactivation and Pi-mediated activation of pyruvate, Pi dikinase. *Arch Biochem Biophys* 237, 490-503.
- 916 Case, D.A., Ben-Shalom, I.Y., Brozell, S.R., Cerutti, D.S., Cheatham Iii, T.E., Cruzeiro, 917 V.W.D., Darden, T.A., Duke, R.E., Ghoreishi, D., Gilson, M.K., Gohlke, H., Goetz, 918 A.W., Greene, D., R Harris, Homeyer, N., Izadi, S., Kovalenko, A., Kurtzman, T., 919 Lee, T.S., Legrand, S., Li, P., Lin, C., Liu, J., Luchko, T., Luo, R., Mermelstein, D.J., 920 Merz, K.M., Miao, Y., Monard, G., Nguyen, C., Nguyen, H., Omelyan, I., Onufriev, 921 A., Pan, F., Qi, R., Roe, D.R., Roitberg, A., Sagui, C., Schott-Verdugo, S., Shen, J., 922 Simmerling, C.L., Smith, J., Salomon-Ferrer, R., Swails, J., Walker, R.C., Wang, J., 923 Wei, H., Wolf, R.M., Wu, X., Xiao, L., York, D.M., and Kollman, P.A. (2018). 924 "AMBER 2018". University of California, San Francisco).
- Case, D.A., Cheatham Iii, T.E., Darden, T., Gohlke, H., Luo, R., Merz Jr, K.M., Onufriev, A.,
 Simmerling, C., Wang, B., and Woods, R.J. (2005). The Amber biomolecular
 simulation programs. *Journal of Computational Chemistry* 26, 1668-1688.
 - Chao, Q., Liu, X.Y., Mei, Y.C., Gao, Z.F., Chen, Y.B., Qian, C.R., Hao, Y.B., and Wang, B.C. (2014). Light-regulated phosphorylation of maize phosphoenolpyruvate carboxykinase plays a vital role in its activity. *Plant Mol Biol* 85, 95-105.

929

930

931

932

933

934

935

936

937

938

939

940

941

942

943

944

- Chastain, C.J., Botschner, M., Harrington, G.E., Thompson, B.J., Mills, S.E., Sarath, G., and Chollet, R. (2000). Further analysis of maize C-4 pyruvate, orthophosphate dikinase phosphorylation by its bifunctional regulatory protein using selective substitutions of the regulatory Thr-456 and catalytic His-458 residues. *Archives of Biochemistry and Biophysics* 375, 165-170.
- Chastain, C.J., Xu, W., Parsley, K., Sarath, G., Hibberd, J.M., and Chollet, R. (2008). The pyruvate, orthophosphate dikinase regulatory proteins of Arabidopsis possess a novel, unprecedented Ser/Thr protein kinase primary structure. *Plant J* 53, 854-863.
- Chen, Y.B., Lu, T.C., Wang, H.X., Shen, J., Bu, T.T., Chao, Q., Gao, Z.F., Zhu, X.G., Wang, Y.F., and Wang, B.C. (2014). Posttranslational Modification of Maize Chloroplast Pyruvate Orthophosphate Dikinase Reveals the Precise Regulatory Mechanism of Its Enzymatic Activity. *Plant Physiol* 165, 534-549.
- Collins, B.C., Gillet, L.C., Rosenberger, G., Rost, H.L., Vichalkovski, A., Gstaiger, M., and Aebersold, R. (2013). Quantifying protein interaction dynamics by SWATH mass spectrometry: application to the 14-3-3 system. *Nat Methods* 10, 1246-1253.
- Detarsio, E., Maurino, V.G., Alvarez, C.E., Muller, G.L., Andreo, C.S., and Drincovich, M.F. (2008). Maize cytosolic NADP-malic enzyme (ZmCytNADP-ME): a phylogenetically distant isoform specifically expressed in embryo and emerging roots. *Plant Mol Biol* 68, 355-367.
- Detarsio, E., Wheeler, M.C., Campos Bermudez, V.A., Andreo, C.S., and Drincovich, M.F.
 (2003). Maize C4 NADP-malic enzyme. Expression in Escherichia coli and characterization of site-directed mutants at the putative nucleoside-binding sites. *J Biol Chem* 278, 13757-13764.
- Dissmeyer, N., and Schnittger, A. (2011). Use of phospho-site substitutions to analyze the biological relevance of phosphorylation events in regulatory networks. *Methods Mol Biol* 779, 93-138.

Dupradeau, F.Y., Cezard, C., Lelong, R., Stanislawiak, E., Pecher, J., Delepine, J.C., and Cieplak, P. (2008). R.E.DD.B.: a database for RESP and ESP atomic charges, and force field libraries. *Nucleic Acids Res* 36, D360-367.

964

965

966

967

968

969

970

971

975

976

977

978

979

980

981

982

983

984

985

986

987

988

989

990

991

992

993

- Fahnenstich, H., Saigo, M., Niessen, M., Zanor, M.I., Andreo, C.S., Fernie, A.R., Drincovich,
 M.F., Flugge, U.I., and Maurino, V.G. (2007). Alteration of organic acid metabolism
 in Arabidopsis overexpressing the maize C(4)NADP-malic enzyme causes accelerated
 senescence during extended darkness. *Plant Physiology* 145, 640-652.
 - Furbank, R.T. (2011). Evolution of the C₄ photosynthetic mechanism: are there really three C₄ acid decarboxylation types? *Journal of Experimental Botany* 62, 3103-3108.
 - Furbank, R.T., and Hatch, M.D. (1987). Mechanism of c(4) photosynthesis: the size and composition of the inorganic carbon pool in bundle sheath cells. *Plant Physiol* 85, 958-964.
 - Furbank, R.T., Jenkins, C.L.D., and Hatch, M.D. (1990). C4 photosynthesis—quantum requirement, C4 acid overcycling and Q-cycle involvement. *Australian Journal of Plant Physiology* 17, 1-7.
- Furumoto, T., Izui, K., Quinn, V., Furbank, R.T., and Von Caemmerer, S. (2007).
 Phosphorylation of phosphoenolpyruvate carboxylase is not essential for high
 photosynthetic rates in the C4 species Flaveria bidentis. *Plant Physiol* 144, 1936-1945.
 - Genheden, S., and Ryde, U. (2015). The MM/PBSA and MM/GBSA methods to estimate ligand-binding affinities. *Expert Opin Drug Discov* 10, 449-461.
 - Gohlke, H., and Case, D.A. (2004). Converging free energy estimates: MM-PB(GB)SA studies on the protein-protein complex Ras-Raf. *Journal of Computational Chemistry* 25, 238-250.
 - Hartwell, J., Gill, A., Nimmo, G.A., Wilkins, M.B., Jenkins, G.I., and Nimmo, H.G. (1999). Phosphoenolpyruvate carboxylase kinase is a novel protein kinase regulated at the level of expression. *Plant J* 20, 333-342.
 - Hatch, M.D. (1987). C-4 Photosynthesis a Unique Blend of Modified Biochemistry, Anatomy and Ultrastructure. *Biochimica Et Biophysica Acta* 895, 81-106.
 - Homeyer, N., Horn, A.H., Lanig, H., and Sticht, H. (2006). AMBER force-field parameters for phosphorylated amino acids in different protonation states: phosphoserine, phosphothreonine, phosphotyrosine, and phosphohistidine. *Journal of molecular modeling* 12, 281-289.
 - Homeyer, N., Stoll, F., Hillisch, A., and Gohlke, H. (2014). Binding Free Energy Calculations for Lead Optimization: Assessment of Their Accuracy in an Industrial Drug Design Context. *Journal of Chemical Theory and Computation* 10, 3331-3344.
 - Hopkins, C.W., Le Grand, S., Walker, R.C., and Roitberg, A.E. (2015). Long-Time-Step Molecular Dynamics through Hydrogen Mass Repartitioning. *Journal of Chemical Theory and Computation* 11, 1864-1874.
- Hornak, V., Abel, R., Okur, A., Strockbine, B., Roitberg, A., and Simmerling, C. (2006).
 Comparison of multiple Amber force fields and development of improved protein
 backbone parameters. *Proteins: Structure, Function, and Bioinformatics* 65, 712-725.
- Hou, T.J., Wang, J.M., Li, Y.Y., and Wang, W. (2011). Assessing the Performance of the MM/PBSA and MM/GBSA Methods. 1. The Accuracy of Binding Free Energy Calculations Based on Molecular Dynamics Simulations. *Journal of Chemical Information and Modeling* 51, 69-82.
- Iglesias, A.A., and Andreo, C.S. (1990). Kinetic and Structural Properties of NADP-Malic Enzyme from Sugarcane Leaves. *Plant Physiol* 92, 66-72.
- 1004 Imaizumi, N., Ku, M.S., Ishihara, K., Samejima, M., Kaneko, S., and Matsuoka, M. (1997). 1005 Characterization of the gene for pyruvate, orthophosphate dikinase from rice, a C3
- plant, and a comparison of structure and expression between C3 and C4 genes for this protein. *Plant Mol Biol* 34, 701-716.

- Ishizaki, K., Larson, T.R., Schauer, N., Fernie, A.R., Graham, I.A., and Leaver, C.J. (2005).

 The critical role of Arabidopsis electron-transfer flavoprotein:ubiquinone oxidoreductase during dark-induced starvation. *Plant Cell* 17, 2587-2600.
- Jiao, J.A., and Chollet, R. (1988). Light/dark regulation of maize leaf phosphoenolpyruvate carboxylase by in vivo phosphorylation. *Arch Biochem Biophys* 261, 409-417.
- Jiao, J.A., and Chollet, R. (1989). Regulatory seryl-phosphorylation of C4
 phosphoenolpyruvate carboxylase by a soluble protein kinase from maize leaves. *Arch Biochem Biophys* 269, 526-535.
- Jiao, J.A., and Chollet, R. (1990). Regulatory phosphorylation of serine-15 in maize
 phosphoenolpyruvate carboxylase by a C4-leaf protein-serine kinase. *Arch Biochem Biophys* 283, 300-305.
- Jorgensen, W.L., Chandrasekhar, J., Madura, J.D., Impey, R.W., and Klein, M.L. (1983).
 Comparison of simple potential functions for simulating liquid water. *The Journal of Chemical Physics* 79, 926-935.
- Kromdijk, J., Ubierna, N., Cousins, A.B., and Griffiths, H. (2014). Bundle-sheath leakiness in C4 photosynthesis: a careful balancing act between CO2 concentration and assimilation. *J Exp Bot* 65, 3443-3457.
- Laemmli, U.K. (1970). Cleavage of structural proteins during the assembly of the head of bacteriophage T4. *Nature* 227, 680-685.
- Lambert, J.P., Ivosev, G., Couzens, A.L., Larsen, B., Taipale, M., Lin, Z.Y., Zhong, Q.,
 Lindquist, S., Vidal, M., Aebersold, R., Pawson, T., Bonner, R., Tate, S., and Gingras,
 A.C. (2013). Mapping differential interactomes by affinity purification coupled with
 data-independent mass spectrometry acquisition. *Nat Methods* 10, 1239-1245.
- Le Grand, S., Gotz, A.W., and Walker, R.C. (2013). SPFP: Speed without compromise-A mixed precision model for GPU accelerated molecular dynamics simulations.

 Computer Physics Communications 184, 374-380.
- Lee, Y., and Fiehn, O. (2008). High quality metabolomic data for Chlamydomonas reinhardtii. *Plant Methods* 4, 7.
- Li, P.F., Roberts, B.P., Chakravorty, D.K., and Merz, K.M. (2013). Rational Design of
 Particle Mesh Ewald Compatible Lennard-Jones Parameters for +2 Metal Cations in
 Explicit Solvent. *Journal of Chemical Theory and Computation* 9, 2733-2748.
- Lisec, J., Schauer, N., Kopka, J., Willmitzer, L., and Fernie, A.R. (2006). Gas chromatography mass spectrometry-based metabolite profiling in plants. *Nat Protoc* 1, 387-396.
- Luis, I.M., Alexandre, B.M., Oliveira, M.M., and Abreu, I.A. (2016). Selection of an Appropriate Protein Extraction Method to Study the Phosphoproteome of Maize Photosynthetic Tissue. *PLoS One* 11, e0164387.
- Miller, B.R., Mcgee, T.D., Swails, J.M., Homeyer, N., Gohlke, H., and Roitberg, A.E. (2012).
 MMPBSA.py: An Efficient Program for End-State Free Energy Calculations. *Journal of Chemical Theory and Computation* 8, 3314-3321.
- Nimmo, H.G. (2000). The regulation of phosphoenolpyruvate carboxylase in CAM plants. *Trends Plant Sci* 5, 75-80.
- Nimmo, H.G. (2003). Control of the phosphorylation of phosphoenolpyruvate carboxylase in higher plants. *Arch Biochem Biophys* 414, 189-196.
- Pastor, R.W., Brooks, B.R., and Szabo, A. (1988). An Analysis of the Accuracy of Langevin and Molecular-Dynamics Algorithms. *Molecular Physics* 65, 1409-1419.
- Roe, D.R., and Cheatham, T.E. (2013). PTRAJ and CPPTRAJ: Software for Processing and Analysis of Molecular Dynamics Trajectory Data. *Journal of Chemical Theory and Computation* 9, 3084-3095.

- Ryckaert, J.P., Ciccotti, G., and Berendsen, H.J.C. (1977). Numerical-Integration of Cartesian Equations of Motion of a System with Constraints - Molecular-Dynamics of N-Alkanes. *Journal of Computational Physics* 23, 327-341.
- Sage, R.F., Sage, T.L., and Kocacinar, F. (2012). Photorespiration and the Evolution of C-4 Photosynthesis. *Annu Rev Plant Biol* 63, 19-47.
- Saigo, M., Alvarez, C.E., Andreo, C.S., and Drincovich, M.F. (2013). Plastidial NADP-malic enzymes from grasses: unraveling the way to the C4 specific isoforms. *Plant Physiol Biochem* 63, 39-48.
- Saigo, M., Bologna, F.P., Maurino, V.G., Detarsio, E., Andreo, C.S., and Drincovich, M.F. (2004). Maize recombinant non-C4 NADP-malic enzyme: a novel dimeric malic enzyme with high specific activity. *Plant Mol Biol* 55, 97-107.
- Schaffner, W., and Weissmann, C. (1973). A rapid, sensitive, and specific method for the determination of protein in dilute solution. *Anal Biochem* 56, 502-514.
- Schuck, P., and Rossmanith, P. (2000). Determination of the sedimentation coefficient distribution by least-squares boundary modeling. *Biopolymers* 54, 328-341.
- Sharwood, R.E., Sonawane, B.V., and Ghannoum, O. (2014). Photosynthetic flexibility in maize exposed to salinity and shade. *J Exp Bot* 65, 3715-3724.
- 1074 Sreerama, N., and Woody, R.W. (2000). Estimation of protein secondary structure from circular dichroism spectra: comparison of CONTIN, SELCON, and CDSSTR methods with an expanded reference set. *Anal Biochem* 287, 252-260.
- Steinbrecher, T., Latzer, J., and Case, D.A. (2012). Revised AMBER Parameters for Bioorganic Phosphates. *Journal of Chemical Theory and Computation* 8, 4405-4412.
- Tan, C., Tan, Y.-H., and Luo, R. (2007). Implicit Nonpolar Solvent Models. *The Journal of Physical Chemistry B* 111, 12263-12274.
- Van Stokkum, I.H., Spoelder, H.J., Bloemendal, M., Van Grondelle, R., and Groen, F.C. (1990). Estimation of protein secondary structure and error analysis from circular dichroism spectra. *Anal Biochem* 191, 110-118.
- Walker, R.P., Chen, Z.H., Acheson, R.M., and Leegood, R.C. (2002). Effects of phosphorylation on phosphoenolpyruvate carboxykinase from the C4 plant Guinea grass. *Plant Physiol* 128, 165-172.
- Walker, R.P., and Leegood, R.C. (1996). Phosphorylation of phosphoenolpyruvate carboxykinase in plants. Studies in plants with C4 photosynthesis and Crassulacean acid metabolism and in germinating seeds. *Biochem J* 317 (Pt 3), 653-658.
- Wang, C., Nguyen, P.H., Pham, K., Huynh, D., Le, T.B., Wang, H., Ren, P., and Luo, R. (2016). Calculating protein-ligand binding affinities with MMPBSA: Method and error analysis. *J Comput Chem* 37, 2436-2446.
- Wang, J.M., Wolf, R.M., Caldwell, J.W., Kollman, P.A., and Case, D.A. (2004).

 Development and testing of a general amber force field. *Journal of Computational Chemistry* 25, 1157-1174.
- Wei, M., Li, Z., Ye, D., Herzberg, O., and Dunaway-Mariano, D. (2000). Identification of domain-domain docking sites within Clostridium symbiosum pyruvate phosphate dikinase by amino acid replacement. *J Biol Chem* 275, 41156-41165.
- Weis, A., Katebzadeh, K., Soderhjelm, P., Nilsson, I., and Ryde, U. (2006). Ligand affinities predicted with the MM/PBSA method: Dependence on the simulation method and the force field. *Journal of Medicinal Chemistry* 49, 6596-6606.
- Whitmore, L., and Wallace, B.A. (2004). DICHROWEB, an online server for protein secondary structure analyses from circular dichroism spectroscopic data. *Nucleic Acids Res* 32, W668-673.
- Zell, M.B., Fahnenstich, H., Maier, A., Saigo, M., Voznesenskaya, E.V., Edwards, G.E.,
- Andreo, C., Schleifenbaum, F., Zell, C., Drincovich, M.F., and Maurino, V.G. (2010).
- Analysis of Arabidopsis with highly reduced levels of malate and fumarate sheds light

1108 1109 1110	on the role of these organic acids as storage carbon molecules. <i>Plant Physiol</i> 152, 1251-1262.
1111	

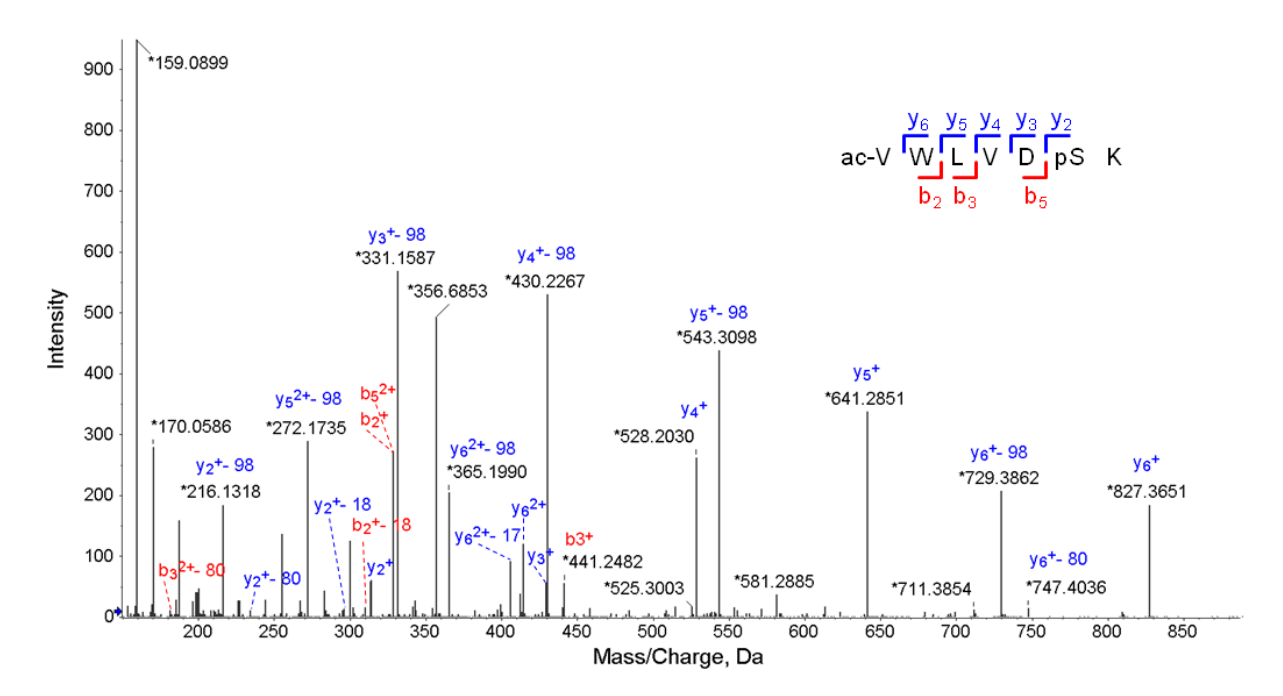
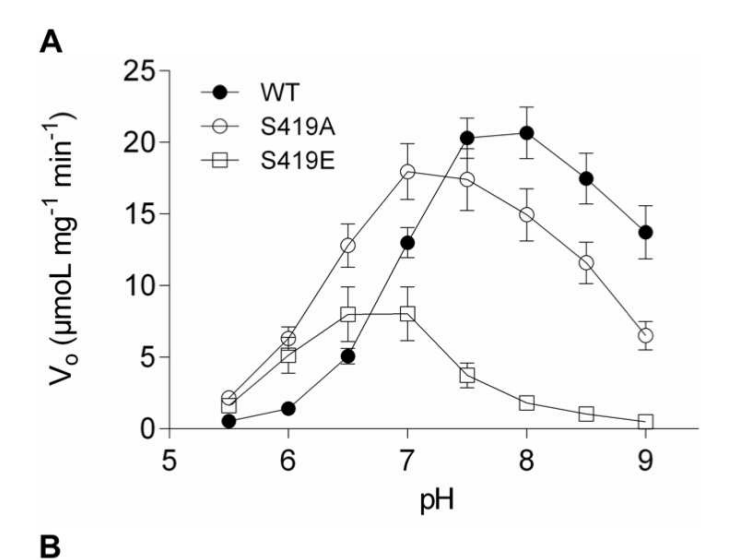


Figure 1. TripleTOF 6600 tandem MS data of the phosphopeptide acVWLVDpSK of ZmC₄-NADP-ME. The detected b (N-terminal, in red) and y (C-terminal, in blue) fragment ions are labeled in the spectrum. Ac denotes N-terminus acetylation and pS denotes phosphorylated serine. Precursor charge: +2; monoisotopic m/z: 484.7265 Da (-1.60 mmu/-3.30 ppm). Confidence (ProteinPilot): 96.4% (Confidence threshold for FDR \leq 1% was equal to 93.7%).



ZmC ₄ -NADP-ME	WT	S419E	S419A
$k_{\text{cat}}(s^{-1})$	12.2 ± 1.4	2.1 ± 0.1*	8.3 ± 1.6
K_{m} NADP (μM)	12.3 ± 0.7	-	159.5 ± 7.5
K _m malate (mM)	0.19 ± 0.01	2.68 ± 0.14*	0.47 ± 0.08

^{-,} non-determined, as saturation was achieved with extremely high NADP concentrations.

Figure 2. Biochemical characterization of recombinant ZmC₄-NADP-ME versions. A, Dependence of the activity, measured using 0.5 mM NADP and 4 mM malate, on the pH of the assay. The values represent the mean \pm standard error of at least four independent enzyme preparations, each measured in triplicate. B, Kinetic parameters at pH 8.0. Kinetic data were best fitted by nonlinear regression analysis. The values represent the mean \pm standard error of at least three independent enzyme preparations, each measured in triplicate.

^{*} Apparent kinetic parameters (k_{catapp} and K_{mapp} malate) of S419E were estimated using a non-saturating NADP concentration of 0.5 mM.

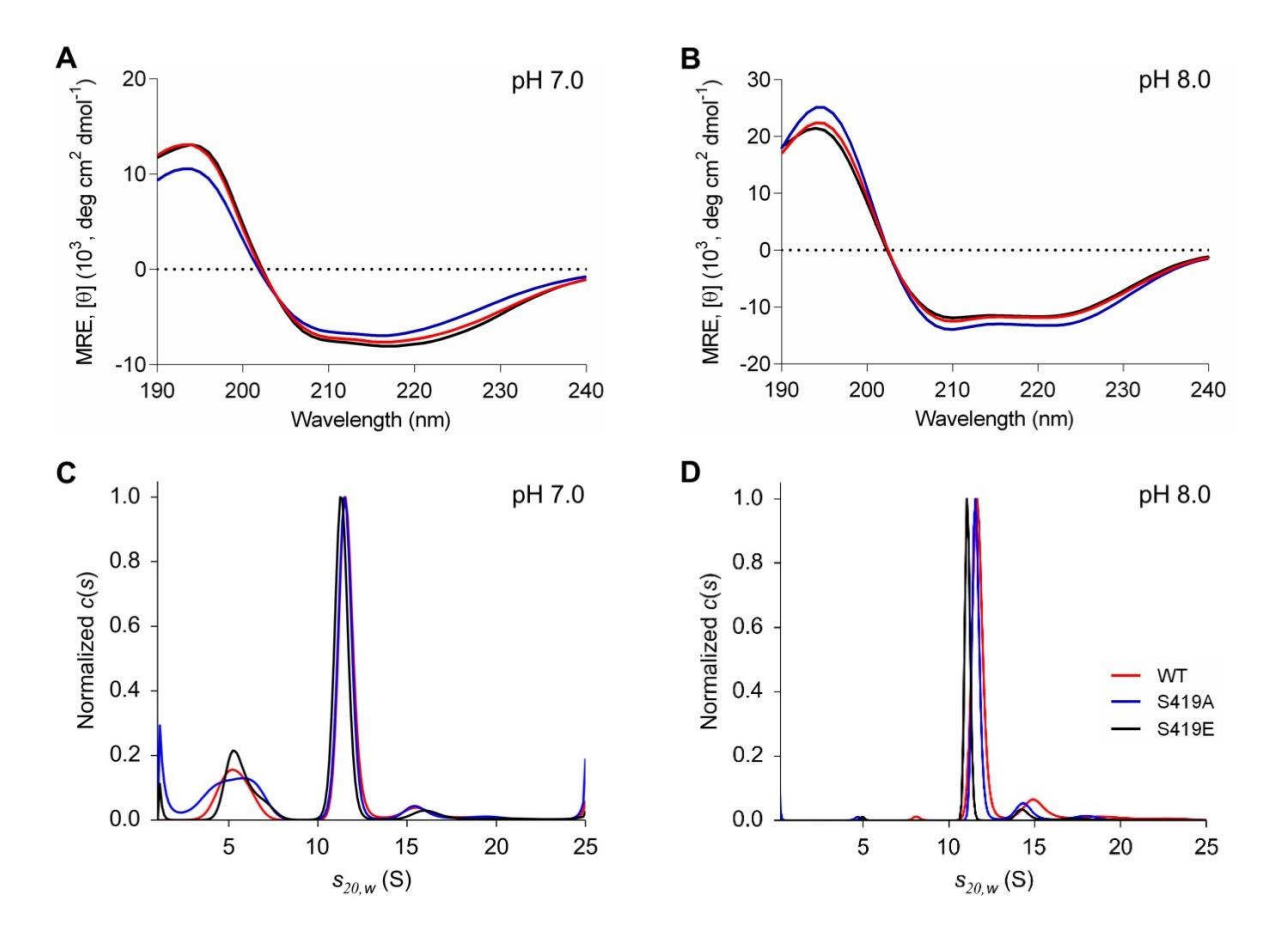


Figure 3. Exploration of the secondary structure organization and quaternary composition of recombinant ZmC₄-NADP-ME versions. A and B: CD spectra of ZmC₄-NADP-ME WT and the two mutated versions obtained at pH 7.0 (A) and 8.0 (B). Ten accumulations each were collected from 190 to 260 nm for 0.16 mg mL⁻¹ enzyme, at 20°C. Each graph is showing the reconstructed curves obtained by applying CONTIN/LL algorithm for data evaluation as provided by the Dichroweb server. **C and D:** Continuous sedimentation coefficient distribution of ZmC₄-NADP-ME WT and the mutated versions at pH 7.0 (C) and 8.0 (D). Data was fitted with the ls-g*(s) model in the software package SEDFIT.

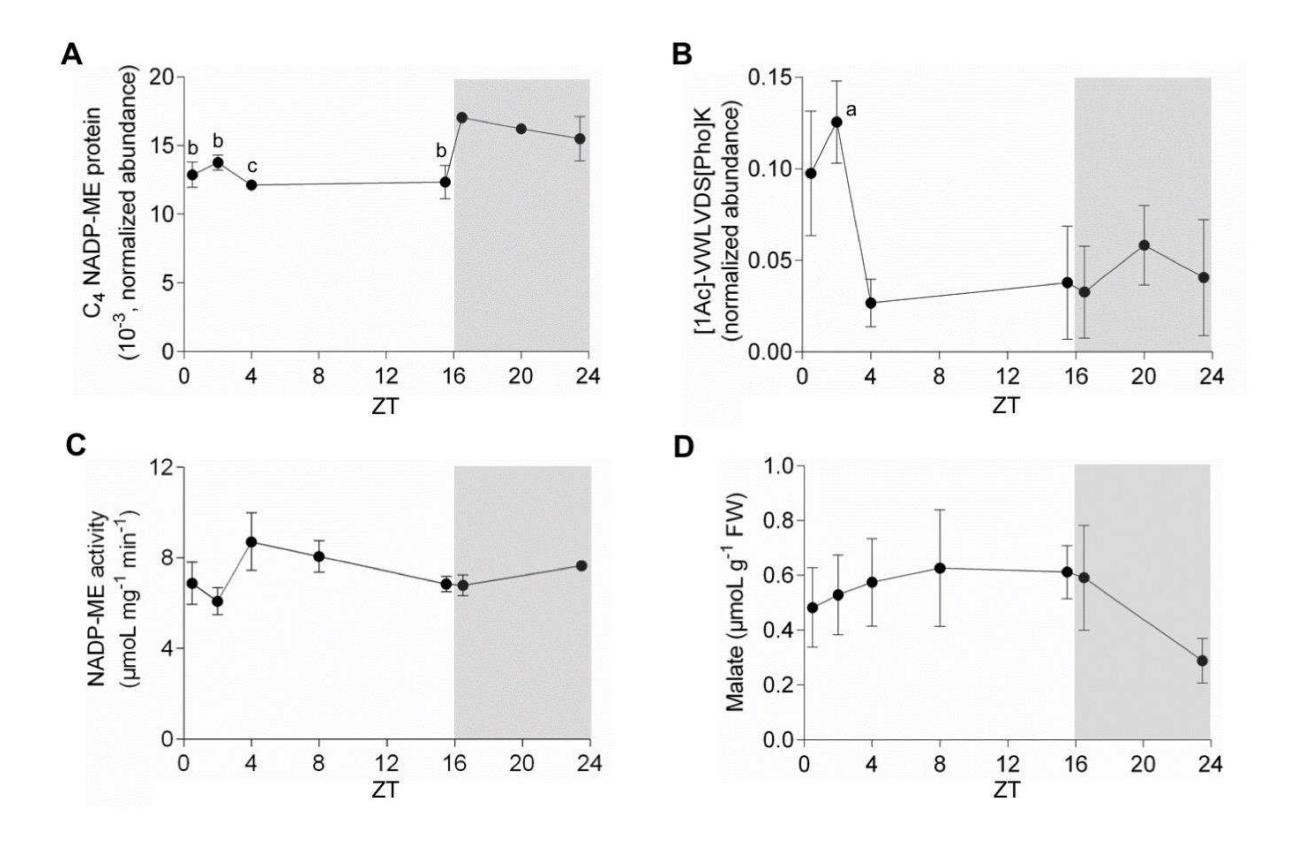


Figure 4. Measurements of different parameters in extracts of maize leaves during a diurnal cycle. A, Quantification of total ZmC₄-NADP-ME protein by SWATH-MS. B, Quantification of the phosphopeptide VWLVDpSK, corresponding to the phosphorylation of ZmC₄-NADP-ME at S419. C, Total NADP-ME activity measured with 1.5 - 2.0 μ g protein extracts. D, Malate concentration assayed by GC-MS analysis. Values represent mean \pm standard error of four (A and B) or three (C and D) biological replicates. The dark period is highlighted in grey. Statistical analyses were performed in all cases (A to D) against the first time point in the night (ZT16.5 = 16.5 h). Letters indicate that the value is statistically significant at a, 0.05; b, 0.01; c, 0.001 levels (the precise p-values are shown in Supplementary Table 3). ZT, Zeitgeber Time.

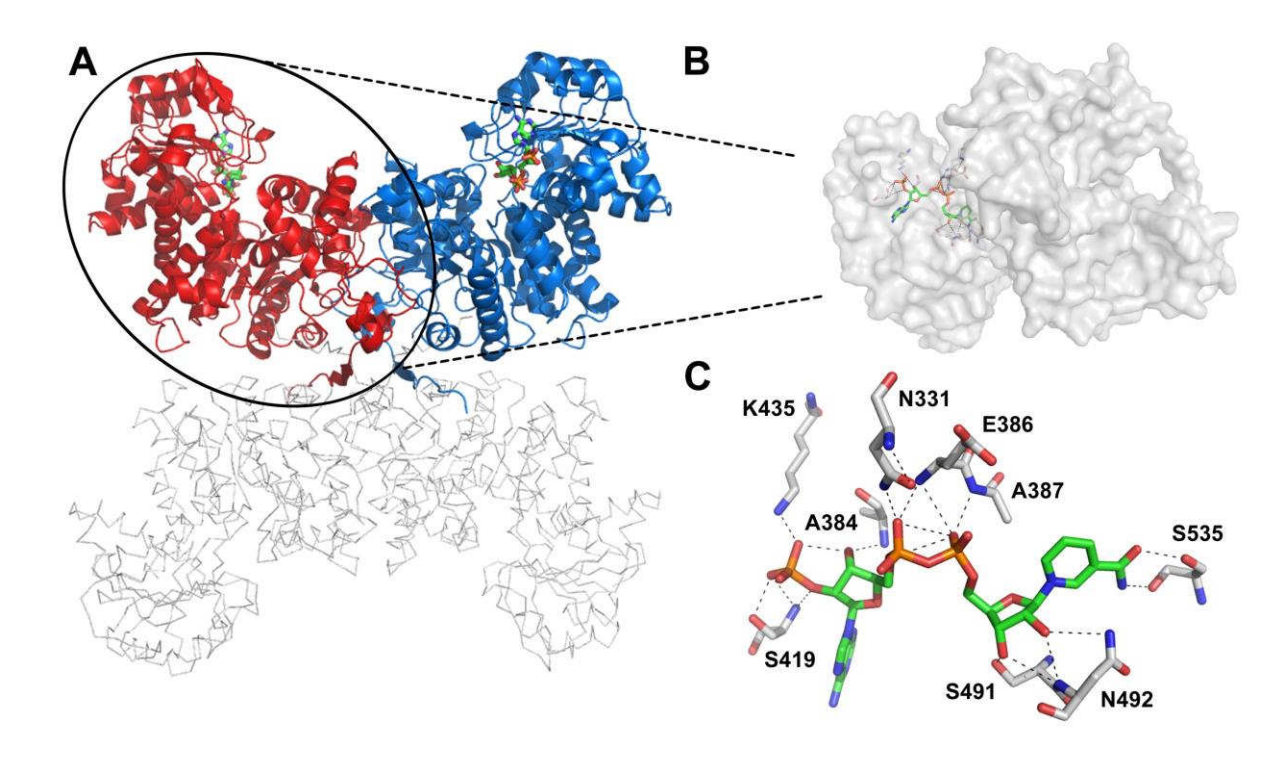


Figure 5. SbC₄-NADP-ME crystal structure and amino acids involved in cofactor binding. A, Cartoon and ribbon representation of SbC₄-NADP-ME. Monomer A (red) and B (blue) with bound cofactor NADP (colored sticks). Large parts of chain C and D are not well resolved by electron density; therefore, we depicted these chains as gray ribbons only to clarify the tetrameric assembly. **B**, Monomer A from SbC₄-NADP-ME as surface representation with the bound cofactor NADP (represented by sticks). **C**, Residues involved in cofactor binding are depicted as sticks with labels (distances are omitted for clarity and are listed in Table S2).

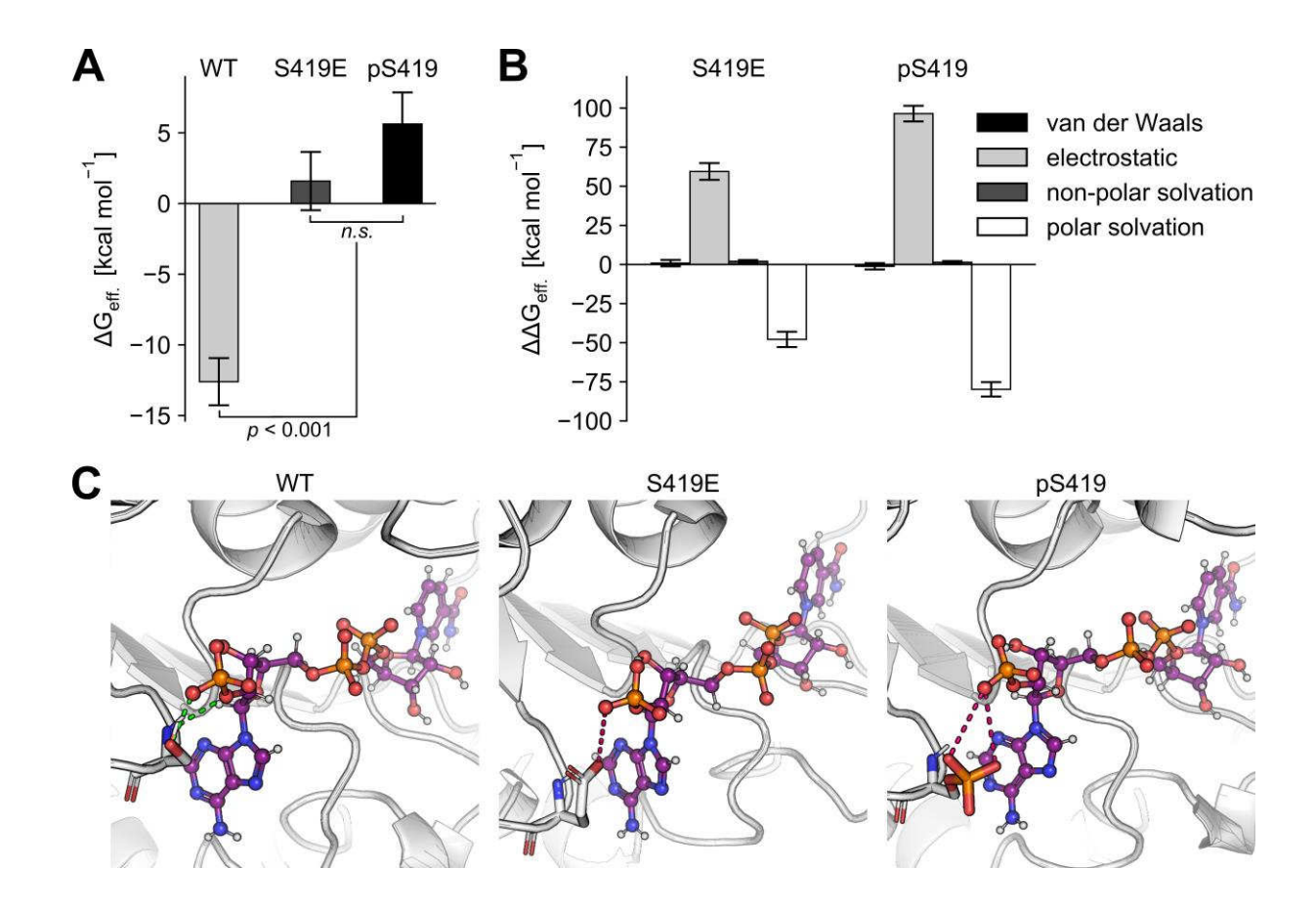


Figure 6: Effective free energies of binding of NADP. A, Effective binding energies computed according to the MM-PBSA approach for WT ZmC₄-NADP-ME, the phosphomimetic variant (S419E), and the phosphorylated enzyme (pS419). The error bars indicate the standard error of the mean over 10 individual trajectories. Statistical significance was calculated according to Student's *t*-test. **B**, The contribution of the different energy terms, computed as variant's energy term minus the respective energy term of the WT enzyme ($\Delta\Delta G_{\text{eff.}} = \Delta G_{\text{eff}}(\text{Var}) - \Delta G_{\text{eff}}(\text{WT})$). Positive terms indicate more favorable binding to the WT enzyme, negative ones to the variant. The error bars show the standard error of the mean of the differences in the individual terms over the trajectories. **C**, Molecular representation of NADP bound to the WT ZmC₄-NADP-ME, the phosphomimetic variant (S419E), and the phosphorylated enzyme (pS419). Interactions with residue 419 are highlighted, showing hydrogen bonds for the WT enzyme with green dashed lines, and charge-charge repulsion for the phosphomimetic and phosphorylated variants with red dashed lines.

Parsed Citations

2019. . "Molecular Operating Environment (MOE)". 2019.01 ed.: Chemical Computing Group ULC, 1010 Sherbooke St. West, Suite #910, Montreal, QC, Canada, H3A2R7). Agarie, S., Kai, M., Takatsuji, H., and Ueno, O. (1997). Expression of C3 and C4 photosynthetic characteristics in the amphibious plant Eleocharis vivipara: structure and analysis of the expression of isogenes for pyruvate, orthophosphate dikinase. Plant Mol Biol 34, 363-369. Avarez, C.E., Bovdilova, A, Höppner, A, Wolff, C.-C., Saigo, M., Trajtenberg, F., Zhang, T., Buschiazzo, A, Nagel-Steger, L., Drincovich, M.F., Lercher, M.J., and Maurino, V.G. (2019). Molecular adaptations of NADPmalic enzyme for its function in C4 photosynthesis in grasses. Nature Plants (in press). Alvarez, C.E., Detarsio, E., Moreno, S., Andreo, C.S., and Drincovich, M.F. (2012). Functional characterization of residues involved in redox modulation of maize photosynthetic NADPmalic enzyme activity. Plant Cell Physiol 53, 1144-1153. Alvarez, C.E., Saigo, M., Margarit, E., Andreo, C.S., and Drincovich, M.F. (2013). Kinetics and functional diversity among the five members of the NADP-malic enzyme family from Zea mays, a C4 species. Photosynth Res 115, 65-80. Amanchy, R., Periaswamy, B., Mathivanan, S., Reddy, R., Tattikota, S.G., and Pandey, A (2007). A curated compendium of phosphorylation motifs. Nat Biotechnol 25, 285-286. Arrivault, S., Obata, T., Szecowka, M., Mengin, V., Guenther, M., Hoehne, M., Fernie, AR., and Stitt, M. (2017). Metabolite pools and carbon flow during C4 photosynthesis in maize: 13CO2 labeling kinetics and cell type fractionation. J Exp Bot 68, 283-298. Astley, H.M., Parsley, K., Aubry, S., Chastain, C.J., Burnell, J.N., Webb, M.E., and Hibberd, J.M. (2011). The pyruvate, orthophosphate dikinase regulatory proteins of Arabidopsis are both bifunctional and interact with the catalytic and nucleotide-binding domains of pyruvate, orthophosphate dikinase. Plant J 68, 1070-1080. Bailey, K.J., Gray, J.E., Walker, R.P., and Leegood, R.C. (2007). Coordinate regulation of phosphoenolpyruvate carboxylase and phosphoenolpyruvate carboxykinase by light and CO2 during C4 photosynthesis. Plant Physiol 144, 479-486. Bayly, C.I., Cieplak, P., Cornell, W., and Kollman, P.A (1993). A wellbehaved electrostatic potential based method using charge restraints for deriving atomic charges: the RESP model. The Journal of Physical Chemistry 97, 10269-10280. Bellasio, C., and Griffiths, H. (2014a). Acclimation to low light by C4 maize: implications for bundle sheath leakiness. Plant Cell Environ 37, 1046-1058. Bellasio, C., and Griffiths, H. (2014b). The operation of two decarboxylases, transamination, and partitioning of C4 metabolic processes between mesophyll and bundle sheath cells allows light capture to be balanced for the maize C4 pathway. Plant Physiol 164, 466-480. Ben-Shalom, I.Y., Pfeiffer-Marek, S., Baringhaus, K.H., and Gohlke, H. (2017). Efficient Approximation of Ligand Rotational and Translational Entropy Changes upon Binding for Use in MM-PBSA Calculations. Journal of Chemical Information and Modeling 57, 170-189. Berendsen, H.J.C., Postma, J.P.M., Van Gunsteren, W.F., Dinola, A, and Haak, J.R. (1984). Molecular dynamics with coupling to an external bath. The Journal of Chemical Physics 81, 3684-3690. Boxall, S.F., Dever, L.V., Knerova, J., Gould, P.D., and Hartwell, J. (2017). Phosphorylation of Phosphoenolpyruvate Carboxylase Is Essential for Maximal and Sustained Dark CO2 Fixation and Core Circadian Clock Operation in the Obligate Crassulacean Acid Metabolism Species Kalanchoe fedtschenkoi. Plant Cell 29, 2519-2536. Brautigam, C.A. (2015). Calculations and Publication-Quality Illustrations for Analytical Ultracentrifugation Data. Methods Enzymol 562, 109-133. Burnell, J.N. (2010). Cloning and characterization of Escherichia coli DUF299: a bifunctional ADP-dependent kinase--Pi-dependent pyrophosphorylase from bacteria. BMC Biochem 11, 1. Burnell, J.N., and Chastain, C.J. (2006). Cloning and expression of maize-leaf pyruvate, Pi dikinase regulatory protein gene. Biochem Biophys Res Commun 345, 675-680. Burnell, J.N., and Hatch, M.D. (1985). Regulation of C4 photosynthesis: purification and properties of the protein catalyzing ADP-mediated inactivation and Pi-mediated activation of pyruvate, Pi dikinase. Arch Biochem Biophys 237, 490-503. Case, D.A, Ben-Shalom, I.Y., Brozell, S.R., Cerutti, D.S., Cheatham lii, T.E., Cruzeiro, V.W.D., Darden, T.A, Duke, R.E., Ghoreishi, D., Gilson, M.K., Gohlke, H., Goetz, AW., Greene, D., R Harris, Homeyer, N., Izadi, S., Kovalenko, A, Kurtzman, T., Lee, T.S., Legrand, S., Li, P., Lin, C., Liu, J., Luchko, T., Luo, R., Mermelstein, D.J., Merz, K.M., Miao, Y., Monard, G., Nguyen, C., Nguyen, H., Omelyan, I., Onufriev, A, Pan, F., Qi, R., Roe, D.R., Roitberg, A, Sagui, C., Schott-Verdugo, S., Shen, J., Simmerling, C.L., Smith, J., Salomon-Ferrer, R., Swails, J., Walker, R.C., Wang, J., Wei, H., Wolf, R.M., Wu, X., Xiao, L., York, D.M., and Kollman, P.A (2018). "AMBER 2018". University of California, San Francisco). Case, D.A, Cheatham Iii, T.E., Darden, T., Gohlke, H., Luo, R., Merz Jr, K.M., Onufriev, A, Simmerling, C., Wang, B., and Woods, R.J. (2005). The Amber biomolecular simulation programs. Journal of Computational Chemistry 26, 1668-1688. Chao, Q., Liu, X.Y., Mei, Y.C., Gao, Z.F., Chen, Y.B., Qian, C.R., Hao, Y.B., and Wang, B.C. (2014). Light-regulated phosphorylation of maize phosphoenolpyruvate carboxykinase plays a vital role in its activity. Plant Mol Biol 85, 95-105. Chastain, C.J., Botschner, M., Harrington, G.E., Thompson, B.J., Mills, S.E., Sarath, G., and Chollet, R. (2000). Further analysis of maize C-4 pyruvate, orthophosphate dikinase phosphorylation by its bifunctional regulatory protein using selective substitutions of the regulatory Thr-456 and catalytic His-458 residues. Archives of Biochemistry and Biophysics 375, 165-170. Chastain, C.J., Xu, W., Parsley, K., Sarath, G., Hibberd, J.M., and Chollet, R. (2008). The pyruvate, orthophosphate dikinase regulatory proteins of Arabidopsis possess a novel, unprecedented Ser/Thr protein kinase primary structure. Plant J 53, 854-863. Chen, Y.B., Lu, T.C., Wang, H.X., Shen, J., Bu, T.T., Chao, Q., Gao, Z.F., Zhu, X.G., Wang, Y.F., and Wang, B.C. (2014). Posttranslational Modification of Maize Chloroplast Pyruvate Orthophosphate Dikinase Reveals the Precise Regulatory Mechanism of Its Enzymatic Activity. Plant Physiol 165, 534-549. Collins, B.C., Gillet, L.C., Rosenberger, G., Rost, H.L., Vichalkovski, A, Gstaiger, M., and Aebersold, R. (2013). Quantifying protein interaction dynamics by SWATH mass spectrometry: application to the 14-3-3 system. Nat Methods 10, 1246-1253. Detarsio, E., Maurino, V.G., Alvarez, C.E., Muller, G.L., Andreo, C.S., and Drincovich, M.F. (2008). Maize cytosolic NADP-malic enzyme (ZmCytNADP-ME): a phylogenetically distant isoform specifically expressed in embryo and emerging roots. Plant Mol Biol 68, 355-367. Detarsio, E., Wheeler, M.C., Campos Bermudez, V.A., Andreo, C.S., and Drincovich, M.F. (2003). Maize C4 NADP-malic enzyme. Expression in Escherichia coli and characterization of site-directed mutants at the putative nucleoside-binding sites. J Biol Chem 278, 13757-13764. Dissmeyer, N., and Schnittger, A (2011). Use of phospho-site substitutions to analyze the biological relevance of phosphorylation events in regulatory networks. Methods Mol Biol 779, 93-138. Dupradeau, F.Y., Cezard, C., Lelong, R., Stanislawiak, E., Pecher, J., Delepine, J.C., and Cieplak, P. (2008). R.E.DD.B.: a database for RESP and ESP atomic charges, and force field libraries. Nucleic Acids Res 36, D360-367. Fahnenstich, H., Saigo, M., Niessen, M., Zanor, M.I., Andreo, C.S., Fernie, A.R., Drincovich, M.F., Flugge, U.I., and Maurino, V.G. (2007). Atteration of organic acid metabolism in Arabidopsis overexpressing the maize C(4)NADP-malic enzyme causes accelerated senescence during extended darkness. Plant Physiology 145, 640-652. Furbank, R.T. (2011). Evolution of the C4 photosynthetic mechanism: are there really three C4 acid decarboxylation types? Journal of Experimental Botany 62, 3103-3108. Furbank, R.T., and Hatch, M.D. (1987). Mechanism of c(4) photosynthesis: the size and composition of the inorganic carbon pool in bundle sheath cells. Plant Physiol 85, 958-964. Furbank, R.T., Jenkins, C.L.D., and Hatch, M.D. (1990). C4 photosynthesis—quantum requirement, C4 acid overcycling and Q-cycle involvement. Australian Journal of Plant Physiology 17, 1-7. Furumoto, T., Izui, K., Quinn, V., Furbank, R.T., and Von Caemmerer, S. (2007). Phosphorylation of phosphoenolpyruvate carboxylase is not essential for high photosynthetic rates in the C4 species Flaveria bidentis. Plant Physiol 144, 1936-1945. Genheden, S., and Ryde, U. (2015). The MM/PBSA and MM/GBSA methods to estimate ligandbinding affinities. Expert Opin Drug Discov 10, 449-461. Gohlke, H., and Case, D.A. (2004). Converging free energy estimates: MM-

```
PB(GB)SA studies on the protein-protein complex Ras-Raf. Journal of Computational Chemistry 25, 238-250. Hartwell, J., Gill, A.,
Nimmo, G.A., Wilkins, M.B., Jenkins, G.I., and Nimmo, H.G. (1999). Phosphoenolpyruvate carboxylase kinase is a novel protein kinase
regulated at the level of expression. Plant J 20, 333-342. Hatch, M.D. (1987). C-4 Photosynthesis - a Unique Blend of Modified
Biochemistry, Anatomy and Ultrastructure. Biochimica Et Biophysica Acta 895, 81-106. Homeyer, N., Horn, A.H., Lanig, H., and Sticht, H.
(2006). AMBER force-field parameters for phosphorylated amino acids in different protonation states: phosphoserine,
phosphothreonine, phosphotyrosine, and phosphohistidine. Journal of molecular modeling 12, 281-289. Homeyer, N., Stoll, F., Hillisch,
A, and Gohlke, H. (2014). Binding Free Energy Calculations for Lead Optimization: Assessment of Their Accuracy in an Industrial Drug
Design Context. Journal of Chemical Theory and Computation 10, 3331-3344. Hopkins, C.W., Le Grand, S., Walker, R.C., and Roitberg,
AE. (2015). Long-Time-Step Molecular Dynamics through Hydrogen Mass Repartitioning. Journal of Chemical Theory and Computation
11, 1864-1874. Hornak, V., Abel, R., Okur, A, Strockbine, B., Roitberg, A, and Simmerling, C. (2006). Comparison of multiple Amber force
fields and development of improved protein backbone parameters. Proteins: Structure, Function, and Bioinformatics 65, 712-725. Hou,
T.J., Wang, J.M., Li, Y.Y., and Wang, W. (2011). Assessing the Performance of the MM/PBSA and MM/GBSA Methods. 1. The Accuracy of
Binding Free Energy Calculations Based on Molecular Dynamics Simulations. Journal of Chemical Information and Modeling 51, 69-82.
Iglesias, AA, and Andreo, C.S. (1990). Kinetic and Structural Properties of NADP-Malic Enzyme from Sugarcane Leaves. Plant Physiol
92, 66-72. Imaizumi, N., Ku, M.S., Ishihara, K., Samejima, M., Kaneko, S., and Matsuoka, M. (1997). Characterization of the gene for
pyruvate, orthophosphate dikinase from rice, a C3 plant, and a comparison of structure and expression between C3 and C4 genes for
this protein. Plant Mol Biol 34, 701-716. Ishizaki, K., Larson, T.R., Schauer, N., Fernie, AR., Graham, I.A, and Leaver, C.J. (2005). The
critical role of Arabidopsis electron-transfer flavoprotein: ubiquinone oxidoreductase during dark-induced starvation. Plant Cell 17.
2587-2600. Jiao, J.A, and Chollet, R. (1988). Light/dark regulation of maize leaf phosphoenolpyruvate carboxylase by in vivo
phosphorylation. Arch Biochem Biophys 261, 409-417. Jiao, J.A., and Chollet, R. (1989). Regulatory seryl-phosphorylation of C4
phosphoenolpyruvate carboxylase by a soluble protein kinase from maize leaves. Arch Biochem Biophys 269, 526-535. Jiao, J.A., and
Chollet, R. (1990). Regulatory phosphorylation of serine-15 in maize phosphoenolpyruvate carboxylase by a C4-leaf protein-serine
kinase. Arch Biochem Biophys 283, 300-305. Jorgensen, W.L., Chandrasekhar, J., Madura, J.D., Impey, R.W., and Klein, M.L. (1983).
Comparison of simple potential functions for simulating liquid water. The Journal of Chemical Physics 79, 926-935. Kromdijk, J.,
Ubierna, N., Cousins, AB., and Griffiths, H. (2014). Bundle-sheath leakiness in C4 photosynthesis: a careful balancing act between CO2
concentration and assimilation. J Exp Bot 65, 3443-3457. Laemmli, U.K. (1970). Cleavage of structural proteins during the assembly of
the head of bacteriophage T4. Nature 227, 680-685. Lambert, J.P., Ivosev, G., Couzens, AL., Larsen, B., Taipale, M., Lin, ZY., Zhong, Q.,
Lindquist, S., Vidal, M., Aebersold, R., Pawson, T., Bonner, R., Tate, S., and Gingras, AC. (2013). Mapping differential interactomes by
affinity purification coupled with data-independent mass spectrometry acquisition. Nat Methods 10, 1239-1245. Le Grand, S., Gotz, AW.,
and Walker, R.C. (2013). SPFP: Speed without compromise-A mixed precision model for GPU accelerated molecular dynamics
simulations. Computer Physics Communications 184, 374-380. Lee, Y., and Fiehn, O. (2008). High quality metabolomic data for Chlamydomonas reinhardtii. Plant Methods 4, 7. Li, P.F., Roberts, B.P., Chakravorty, D.K., and Merz, K.M. (2013). Rational Design of
Particle Mesh Ewald Compatible Lennard-Jones Parameters for +2 Metal Cations in Explicit Solvent. Journal of Chemical Theory and
Computation 9, 2733-2748. Lisec, J., Schauer, N., Kopka, J., Willmitzer, L., and Fernie, AR. (2006). Gas chromatography mass
spectrometry-based metabolite profiling in plants. Nat Protoc 1, 387-396. Luis, I.M., Alexandre, B.M., Oliveira, M.M., and Abreu, I.A.
(2016). Selection of an Appropriate Protein Extraction Method to Study the Phosphoproteome of Maize Photosynthetic Tissue. PLoS
One 11, e0164387. Miller, B.R., Mcgee, T.D., Swails, J.M., Homeyer, N., Gohlke, H., and Roitberg, AE. (2012). MMPBSApy: An Efficient
Program for End-State Free Energy Calculations. Journal of Chemical Theory and Computation 8, 3314-3321. Nimmo, H.G. (2000). The
regulation of phosphoenolpyruvate carboxylase in CAM plants. Trends Plant Sci 5, 75-80. Nimmo, H.G. (2003). Control of the
phosphorylation of phosphoenolpyruvate carboxylase in higher plants. Arch Biochem Biophys 414, 189-196. Pastor, R.W., Brooks, B.R.,
and Szabo, A (1988). An Analysis of the Accuracy of Langevin and Molecular-Dynamics Algorithms. Molecular Physics 65, 1409-1419.
Roe, D.R., and Cheatham, T.E. (2013). PTRAJ and CPPTRAJ: Software for Processing and Analysis of Molecular Dynamics Trajectory
Data. Journal of Chemical Theory and Computation 9, 3084-3095. Ryckaert, J.P., Ciccotti, G., and Berendsen, H.J.C. (1977). Numerical-
Integration of Cartesian Equations of Motion of a System with Constraints - Molecular-Dynamics of N-Alkanes. Journal of
Computational Physics 23, 327-341. Sage, R.F., Sage, T.L., and Kocacinar, F. (2012). Photorespiration and the Evolution of C-4
Photosynthesis. Annu Rev Plant Biol 63, 19-47. Saigo, M., Alvarez, C.E., Andreo, C.S., and Drincovich, M.F. (2013). Plastidial NADP-malic
enzymes from grasses: unraveling the way to the C4 specific isoforms. Plant Physiol Biochem 63, 39-48. Saigo, M., Bologna, F.P.,
Maurino, V.G., Detarsio, E., Andreo, C.S., and Drincovich, M.F. (2004). Maize recombinant non-C4 NADP-malic enzyme: a novel dimeric
malic enzyme with high specific activity. Plant Mol Biol 55, 97-107. Schaffner, W., and Weissmann, C. (1973). A rapid, sensitive, and
specific method for the determination of protein in dilute solution. Anal Biochem 56, 502-514. Schuck, P., and Rossmanith, P. (2000).
Determination of the sedimentation coefficient distribution by least-squares boundary modeling. Biopolymers 54, 328-341. Sharwood,
R.E., Sonawane, B.V., and Ghannoum, O. (2014). Photosynthetic flexibility in maize exposed to salinity and shade. J Exp Bot 65, 3715-
3724. Sreerama, N., and Woody, R.W. (2000). Estimation of protein secondary structure from circular dichroism spectra: comparison of
CONTIN, SELCON, and CDSSTR methods with an expanded reference set. Anal Biochem 287, 252-260. Steinbrecher, T., Latzer, J., and
Case, D.A. (2012). Revised AMBER Parameters for Bioorganic Phosphates. Journal of Chemical Theory and Computation 8, 4405-4412.
Tan, C., Tan, Y.-H., and Luo, R. (2007). Implicit Nonpolar Solvent Models. The Journal of Physical Chemistry B 111, 12263-12274. Van
Stokkum, I.H., Spoelder, H.J., Bloemendal, M., Van Grondelle, R., and Groen, F.C. (1990). Estimation of protein secondary structure and
error analysis from circular dichroism spectra, Anal Biochem 191, 110-118, Walker, R.P., Chen, Z.H., Acheson, R.M., and Leggod, R.C.
(2002). Effects of phosphorylation on phosphoenolpyruvate carboxykinase from the C4 plant Guinea grass. Plant Physiol 128, 165-172.
Walker, R.P., and Leegood, R.C. (1996). Phosphorylation of phosphoenolpyruvate carboxykinase in plants. Studies in plants with C4
photosynthesis and Crassulacean acid metabolism and in germinating seeds. Biochem J 317 (Pt 3), 653-658. Wang, C., Nguyen, P.H.,
Pham, K., Huynh, D., Le, T.B., Wang, H., Ren, P., and Luo, R. (2016). Calculating protein-ligand binding affinities with MMPBSA: Method
and error analysis. J Comput Chem 37, 2436-2446. Wang, J.M., Wolf, R.M., Caldwell, J.W., Kollman, P.A, and Case, D.A (2004).
Development and testing of a general amber force field. Journal of Computational Chemistry 25, 1157-1174. Wei, M., Li, Z, Ye, D.,
Herzberg, O., and Dunaway-Mariano, D. (2000). Identification of domain-domain docking sites within Clostridium symbiosum pyruvate
phosphate dikinase by amino acid replacement. J Biol Chem 275, 41156-41165. Weis, A, Katebzadeh, K., Soderhjelm, P., Nilsson, I., and
Ryde, U. (2006). Ligand affinities predicted with the MM/PBSA method: Dependence on the simulation method and the force field.
Journal of Medicinal Chemistry 49, 6596-6606. Whitmore, L., and Wallace, B.A. (2004). DICHROWEB, an online server for protein
secondary structure analyses from circular dichroism spectroscopic data. Nucleic Acids Res 32, W668-673. Zell, M.B., Fahnenstich, H.,
Maier, A, Saigo, M., Voznesenskaya, E.V., Edwards, G.E., Andreo, C., Schleifenbaum, F., Zell, C., Drincovich, M.F., and Maurino, V.G.
(2010). Analysis of Arabidopsis with highly reduced levels of malate and fumarate sheds light on the role of these organic acids as
```

storage carbon molecules. Plant Physiol 152, 1251-1262.

Pubmed: Author and Title
Google Scholar: Author Only Title Only Author and Title